Title: **Intercellular Mitochondrial Transfer as a Rescue Mechanism in Response to Protein Import Failure**

Authors: Hope I Needs[1], Gonçalo C. Pereira[1*], Emily Glover[1], Alina Witt[2], Wolfgang Hübner[2], Mark P. Dodding[1], Jeremy M Henley[1,†] and Ian Collinson[1,†]

Affiliations:

[1] *School of Biochemistry, University of Bristol, Bristol BS8 1TD, UK*

[2] *Fakultät für Physik, Universität Bielefeld, Postfach 100131 D-33501, Germany*

[†], corresponding authors: ian.collinson@bristol.ac.uk and J.M.Henley@bristol.ac.uk

[*], present address: *MRC - Mitochondrial Biology Unit, University of Cambridge, The Keith Peters Building, Cambridge Biomedical Campus, Cambridge CB2 0XY, UK*

Abstract: 125 (100 – 125)

Mitochondria are the powerhouses of eukaryotic cells, composed mostly of nuclear-encoded proteins imported from the cytosol. Thus, problems with the import machinery will disrupt their regenerative capacity and the cell's energy (ATP) supplies–particularly troublesome for energy demanding cells like neurons and myocytes. Unsurprisingly then, dysfunctional import is implicated in disease. This study explores the consequences of import failure in mammalian cells; wherein, blocking the import machinery has profound effects on mitochondrial ultra-structure and dynamics, but, surprisingly, does not impact import. The explanation is an astonishing response involving intercellular mitochondrial transfer *via* tunnelling nanotubes: for the import of healthy mitochondria and jettisoning of those with jammed import sites. These observations support the existence of a widespread mechanism for the rescue of mitochondrial protein import failure.

One-Sentence Summary: 125/ 125 characters

A mitochondrial import rescue mechanism involving intercellular mitochondrial transport through tunneling nanotubes (TNTs).

Main Text:

Mitochondria are semi-autonomous organelles, found inside eukaryotic cells, responsible for oxidative phosphorylation and metabolic regulation amongst other functions. Their small genome encodes only a few proteins (13 in humans) while the remaining proteome (>1000 proteins) is synthesised in the cytosol and imported *via* highly specialised protein translocation machineries. The major route is the presequence pathway, taken by precursor proteins usually (~70%) with cleavable N-terminal mitochondrial targeting sequences (MTS) [1]. These proteins are recognised at the surface of the outer mitochondrial membrane (OMM) by receptors of the translocase of the outer membrane (TOM) complex. Transport then proceeds through the TOM40 channel into the intermembrane space (IMS), towards the translocase of the inner membrane 23 (TIM23) complex [2, 3]. Additional internal sorting sequences are also deployed, which target the translocating precursor through the $TIM23^{SORT}$ complex to be inserted laterally into the inner mitochondrial membrane (IMM) [2]. Otherwise, transport proceeds across the IMM and into the matrix *via* the $TIM23^{MOTOR}$ complex. Passage of proteins into and across the IMM both require the membrane potential ($\Delta\Psi$), while pulling the protein into the matrix also requires ATP turnover [2]. MTS cleavage then enables release, folding, and assembly of the mature protein.

The consequences of mitochondrial import dysfunction, and thereby biogenic failure, are catastrophic for cell health; particularly for high energy consuming cells such as those of muscle and nervous tissue. Indeed, there are strong links between mitochondrial import failure and neurodegeneration, see [4] and references therein. Deficient import leads to the build-up of cytosolic precursor proteins, inducing the inhibition of protein synthesis, activation of the proteasome, and mitoprotein-induced stress responses [5-9]. While these responses have been shown to mitigate against the potential toxic effects of large quantities of aggregation prone precursor, they do not always successfully resolve the underlying problem of cells incapable of mitochondrial regeneration. To maintain overall bioenergetic function, mitochondria with failing import sites either need to be rectified or replaced. This paper describes a remarkable rescue mechanism in cells subject to perturbation of the mitochondrial import machinery. This response invokes the formation of tunneling nanotubes (TNTs), enabling intercellular mitochondrial transport to transfer viable mitochondria from heathy cells to replace defective mitochondria in compromised cells, as well as transferring compromised mitochondria into neighboring healthy cells.

There are multiple possible causes of mitochondrial import failure. Age, exposure to environmental and endogenous (*e.g.* reactive oxygen species–ROS) toxins, as well as nuclear and mitochondrial mutations can all impair bioenergetic function, resulting in depletion of $\Delta\Psi$ and ATP required for import. Additionally, the TOM and TIM complexes can become blocked, *e.g.,* by stalled/misfolded precursor proteins. Indeed, refined kinetic analysis of protein translocation through the mitochondrial import and bacterial secretion machineries [3, 10, 11] show that transport failure and blockages are an integral

component of the reaction cycle. Another possibility is that aggregation prone proteins, such as those variants implicated in neurodegenerative disease (amyloid precursor protein, alpha-synuclein, Huntingtin, and Tau) associate with the import machinery and perturb the transport process [12-14].

To study the consequences of import failure, and the response, we established tools to monitor and artificially block mitochondrial protein import in intact cells. HeLa cells were conditioned in galactose (HeLaGAL) to maximise their dependency on mitochondrial oxidative phosphorylation, in contrast to those grown in glucose (HeLaGLU), which favour glycolytic metabolism [15]. These cells were then utilised to study the impact of precursor stalling. Precursor proteins are imported in an unfolded state, so the C-terminal fusion of dihydrofolate reductase (DHFR), which resists unfolding when bound to the drug methotrexate (MTX), can be exploited to block the import machinery (Fig. 1A) [16, 17]. We therefore engineered a precursor construct encoding the MTS of the ATP synthase Subunit 9 (Su9) fused to a fluorescent reporter protein (EGFP or mScarlet) and DHFR for overexpression in HeLaGAL cells. Imaging and biochemical analysis confirmed that the mature protein was successfully targeted to mitochondria in the absence of MTX, but to a much lesser extent in its presence (Fig. 1A; S1 and S2). Interestingly, within the same cell, structured illumination microscopy (SIM) showed that some mitochondria (43%) were enveloped by aggregated precursor protein, while others were not (Fig. 1B–white and yellow arrows, respectively; S3 and S4).

High-resolution SIM revealed that artificial precursor trapping elicited a profound change in mitochondrial morphology (Fig. 1C; S5). The mitochondria became less branched, more rounded, and increased in width, indicative of fragmentation (Fig. 1C; S6). These effects did not occur when the precursor construct was not transfected, so they were not due to exposure of the drug MTX (Fig. 1C; S5 and S6; NT +MTX). We next analysed the abundance of a known regulator of mitochondrial fission, DRP1, which assembles into spiral-like oligomers when recruited to the OMM. Constriction brings about fission, mediated by GTP hydrolysis [18] and regulated by various post-translational modifications, including phosphorylation of DRP1 at serine616 (p-DRP1 S616) [19]. Western blotting showed that the abundance of total DRP1 was unchanged in HeLaGAL cells following mitochondrial precursor stalling, but phosphorylation at the pro-fission site S616 was increased (Fig. 1D; S7). Thus, we conclude that enhanced mitochondrial fission caused by precursor stalling accounts for the observed morphological changes.

We previously developed a split luciferase assay to monitor protein import into isolated yeast mitochondria [20], which we successfully adapted to our HeLa cell system [21]. Briefly, HeLa cells were cultured with the large fragment of the luciferase (11S) segregated in the mitochondrial matrix, so that the import of a precursor with the small fragment (pep86–required for luminescence) fused to the C-terminus can be monitored. This new capability enabled the reporting of the import of another precursor in HeLaGAL cells subject to precursor stalling by DHFR-MTX, after plasma membrane permeabilisation.

We first tested import dynamics after chronic exposure to precursor stalling (48 hours of *su9-mScarlet-DHFR* overexpression +MTX; see above). Surprisingly, we observed no effect on the import of a second precursor protein *Su9-EGFP-pep86* in our in-cell (HeLaGAL) assay (Fig. 1E–left). However, under more acute stalling conditions *via* the addition of high concentrations of purified precursor protein-DHFR fusion in the presence of MTX and NADPH (for increased stabilisation of DHFR) for 10 minutes, the import of the reporter precursor was diminished (Fig. 1E–middle). Since analogous treatments of isolated mitochondria *in vitro* completely blocked the import sites [3], the preservation of mitochondrial import inside cells following chronic precursor trapping was unexpected. Based on these findings we hypothesised that a clearance or rescue mechanism must be operating, but lost following mitochondrial isolation.

We observed that the cells subject to chronic exposure to precursors with DHFR and MTX (chronic precursor import stalling), exhibited a dramatic increase in thin elongated protrusions (Fig. 2A; S8). The increase in protrusions was dependent on DHFR-induced precursor stalling, and not an off-target effect of MTX, because they were not apparent when the MTS was omitted. Furthermore, this occurrence was dependent on galactose conditioning, confirming the response is mediated by mitochondria [15] (Fig. 2B; S8). Immunocytochemistry and confocal microscopy showed that the protrusions contain microtubules and actin (Fig. 2C), characteristic of tunnelling nanotubes (TNTs), capable of organellar (including mitochondrial) transport between cells [22-25]. To further investigate the identity of these protrusions, cells were treated with nocodazole, which impairs TNT establishment through inhibition of microtubule formation [26-30]. In doing so, the number of protrusions was indeed reduced to the baseline levels (Fig. 2D; S9), consistent with their identity as such.

We next investigated whether these TNTs could be capable of intercellular mitochondrial transport to recruit functional mitochondria, or remove those that have become compromised. Close inspection by super-resolution imaging highlighted the presence of mitochondria inside tubes connecting a cell challenged by precursor stalling with an untransfected healthy cell (Fig. 3A). To confirm mitochondria were transferred between cells, co-cultures of challenged HeLaGAL cells (producing a stalling precursor and a green mitochondrial marker: *Su9-EGFP*) and healthy cells (producing a red mitochondrial marker protein: *Cox8a-DsRed*) were established in the presence of MTX, and imaged by confocal microscopy. The results clearly identified cells containing a mixture of mitochondria originating from both healthy and challenged cells (Fig. 3B). Furthermore, live cell light-sheet fluorescence microscopy showed healthy mitochondria (without precursor stalling) being transferred through a TNT towards a challenged cell (Fig. 3C; supplementary Movie S1). This observation explains why, within a cell exposed to precursor trapping, some mitochondria are surrounded by aggregated precursors, and thereby stalled, while others in the same cell are not (Fig. 1B; S4), the latter potentially originating from TNT connected healthy cells.

Further analysis by confocal microscopy identified TNTs containing healthy mitochondria, travelling from a healthy cell to a cell with trapped precursor (Fig. 3D; example 1). Conversely though, there were

other instances where TNTs were observed containing mitochondria originating from cells with trapped precursor (Fig. 3D; example 2). Thus, it appears that mitochondria travel in both directions; potentially for replenishment from healthy cells, and for affected cells to jettison impaired mitochondria. Interestingly, while mitochondria with trapped precursors are subject to TNT transport, cytosolic precursor proteins accumulated in the cytosol are not – suggesting transport occurs actively, rather than passively by diffusion.

To explore whether this process is a general response to perturbation of the protein import apparatus, HeLa cells were exposed to MitoBloCK-20 (MB20) – a small molecule inhibitor of the presequence pathway acting on TIM17, a key component of the TIM23 complex [31]. Similar to precursor stalling, only acute exposure to the drug affected protein import activity (Fig. 4A). The failure of chronic drug exposure to impact protein import coincides with a large increase in the proportion of cells with structures resembling TNTs (Fig. 4B; S10); once again this only occurred in cells dependent on mitochondria for ATP synthesis (HeLaGAL). These TNTs, induced by chemical inhibition, also contained actin, microtubules, and mitochondria (Fig. S11).

The results presented so far suggest that the TNTs are part of a widespread rescue mechanism that enables cells containing mitochondria with compromised import to receive functional mitochondria from nearby healthy cells, and unload dysfunctional mitochondria for degradation/regeneration. To test this hypothesis, we re-examined protein import, which was apparently unaffected in cells subjected to chronic precursor stalling (Fig. 1E), but in the presence of TNT inhibitor nocodazole. In cells exposed to chronic precursor trapping and treated with nocodazole, we observed a reduction in the total amount of protein imported compared to cells without trapped precursor (Fig. 4C; S12). Therefore, the unexpected resilience of import function, within cells subject to precursor trapping, is dependent on TNTs.

To investigate this rescue mechanism further we deployed tandem mass tagging mass spectrometry (TMT-MS) to identify proteins associated with the trapped precursor. Cells were subject to stalling again through production of a *Su9-EGFP-DHFR* fusion (with and without the MTS and MTX as controls). Following a chronic (48 hour) treatment, mitochondria from HeLaGAL cells were isolated and proteins gently extracted with glyco-diosgenin amphiphile (GDN). Proteins interacting with the precursor were then isolated using a GFP-trap, which effectively binds the precursor (Fig. 4D; S13). TMT-MS analysis of the captured precursor and its associates shows a significant enhancement of proteins when derived from cells cultured in the presence, compared to those in the absence, of MTX. The volcano plot (Fig. 4D; supplementary Table S1) highlights proteins in complex with the stalled precursor (+MTX), controlled against those associated with the imported form (-MTX).

Of the significant hits with >2 fold enhancement, cell adhesion protein fibronectin (FN1) has been shown to be critical for TNT formation and activity [32], whilst apoptosis inducing factor mitochondria associated 2 (AIFM2) is related to mitochondrial import stress signalling [33], and is induced by p53 activity [34] which can induce TNT formation [35]. Interestingly, there is also an enhancement of calcium

signalling proteins Calcium/calmodulin-dependent protein kinase type II subunit delta (CamKIID) and S100A2. Calcium signalling *via* the Ca^{2+}/Wnt pathway has been shown to regulate TNTs previously [36]. Additionally, cytoskeleton related proteins required for TNT formation, such as Microtubule associated protein 4 (MAP4) and Cdc42 effector protein 1 (CDC42EP1), were enhanced [37-39].

Additionally, associated proteins include several proteins involved in stress response pathways, particularly associated with the proteasome (*e.g.,* E3 ubiquitin ligase TRIM25 [40], Proteasome subunit β type 5 (PSMB5) [41], and Heat shock cognate 71 kDa protein (HSPA8) [42, 43]), suggesting that other mitoprotein-induced stress response pathways are also at play. An experiment was also conducted without an MTS to show the non-specific effects of MTX (Fig. S14). In this control there was only one significant enhancement in the presence of MTX (not present in +MTS +MTX); therefore, the hits identified as significantly enhanced represent true associations with the trapped precursor.

Taken together, our results demonstrate that impaired mitochondrial import, be it precursor stalling at the outer membrane or inhibition of the TIM23 complex, invokes a rescue mechanism involving the intercellular transport of mitochondria *via* filamentous, membranous protrusions: TNTs that contain F-actin and microtubules. TNTs have been described previously for their involvement in long-range intercellular communication and transport; including of lipids, nucleic acids, microRNAs, ions such as calcium, fragmented plasma membrane, viruses (*e.g.* coronaviruses) [44] and even entire organelles: mitochondria, ER, Golgi, and endosomes [22-25, 45, 46]. The dimensions of TNTs seem to be tailored according to the cargo, with distinct thin and thick varieties, the latter with a diameter of 1-7 μm, such as those seen here for mitochondrial transport [47-49]. TNT formation can be induced by various stress factors including H_2O_2, serum depletion, mitochondrial stress, and cytotoxicity, which may act *via* the p53 pathway [35]; they alleviate cellular stress by enabling replenishment and/or removing harmful debris. Indeed, healthy mitochondria have previously been reported to transport through TNTs and rescue cells in the early stages of apoptosis [39]. Another study demonstrated that TNTs can assist in reducing cellular toxicity caused by alpha-synuclein fibrils (implicated in Parkinson's disease) in microglia, by facilitating the removal of protein aggregates and the delivery of healthy mitochondria [50]. Here, we show how direct mitochondrial import impairment leads to bidirectional mitochondrial transfer *via* TNTs, suggestive of a widespread mechanism for rescue of mitochondrial function.

It makes sense that the TNT response described, triggered by failing import, helps resolve potentially catastrophic incapacitated mitochondrial biogenesis. Beyond that, we also speculate that the TOM and TIM23 complexes act as reporters of mitochondrial health; whereby, for whatever reason, reduced bioenergetic function would lead to diminished $\Delta\psi$ and/ or ATP, decreasing import efficiency and hence initiating rescue *via* TNTs. In this respect, the connection between protein aggregation associated with neurodegeneration and mitochondrial import is particularly intriguing. Indeed, the intercellular transport of the Tau protein and β-amyloid, associated with Alzheimer's disease, can also occur *via* TNTs [51]. This

could be connected to the propensity of these aggregation prone proteins to associate with the mitochondrial import machinery. Variants of the Huntingtin protein, the causative agent of disease, and the β-amyloid precursor APP have both been shown to associate with the TOM40/TIM23 complexes [12, 14, 52]. Indeed, in a parallel study we show that the a Tau variant linked with neurodegeneration associates with TOM40 and brings about TNT formation [53]. Therefore, these proteins may also act through binding to and impairing the import machinery, inducing TNT formation for aggregate efflux [54-56]. On a more sinister note, perhaps this mechanism could be hijacked to spread infectious agents; whereby viruses or prions target themselves to the mitochondrial import machinery and ride in, through TNTs, to other cells [44, 57, 58].

What emerges from our study is a picture of an astonishing process for rescue of mitochondrial import function involving intercellular mitochondrial transport through TNTs (Fig. 4E). It may well be one of many rescue mechanisms instigated by perturbation of the import apparatus, including the stress response to unfolded precursors in the cytosol [5, 6]. It will be very interesting to see how this mechanism is manifested *in vivo*, to what extent and for what purpose, since mitochondrial import dysfunction underpins a wide range of devastating and often fatal diseases [4, 59, 60]. Greater understanding of the formation and functions of TNTs will provide exciting opportunities for biological engineering and for medical applications. For example, modulating this process genetically, or with small molecules, as we have demonstrated, could enable targeted mitochondrial transport *in vivo*, and approaches to mitochondrial replacement therapy for cell and tissue regeneration.

References and Notes

1. Vogtle, F.N., et al., *Global Analysis of the Mitochondrial N-Proteome Identifies a Processing Peptidase Critical for Protein Stability.* Cell, 2009. **139**(2): p. 428-439.
2. Chacinska, A., et al., *Importing Mitochondrial Proteins: Machineries and Mechanisms.* Cell, 2009. **138**(4): p. 628-644.
3. Ford, H.C., et al., *Towards a molecular mechanism underlying mitochondrial protein import through the TOM and TIM23 complexes.* Elife, 2022. **11**.
4. Needs, H.I., et al., *Interplay between Mitochondrial Protein Import and Respiratory Complexes Assembly in Neuronal Health and Degeneration.* Life-Basel, 2021. **11**(5).
5. Wrobel, L., et al., *Mistargeted mitochondrial proteins activate a proteostatic response in the cytosol.* Nature, 2015. **524**(7566): p. 485-+.
6. Wang, X.W. and X.J. Chen, *A cytosolic network suppressing mitochondria-mediated proteostatic stress and cell death.* Nature, 2015. **524**(7566): p. 481-+.
7. Samluk, L., P. Chroscicki, and A. Chacinska, *Mitochondrial protein import stress and signaling.* Current Opinion in Physiology, 2018. **3**: p. 41-48.
8. Weidberg, H. and A. Amon, *MitoCPR-A surveillance pathway that protects mitochondria in response to protein import stress.* Science, 2018. **360**(6385): p. 10.
9. Martensson, C.U., et al., *Mitochondrial protein translocation-associated degradation.* Nature, 2019. **569**(7758): p. 679-+.
10. Allen, W.J., et al., *Rate-limiting transport of positively charged arginine residues through the Sec-machinery is integral to the mechanism of protein secretion.* Elife, 2022. **11**: p. 23.

11. Allen, W.J., et al., *Refined measurement of SecA-driven protein secretion reveals that translocation is indirectly coupled to ATP turnover.* Proceedings of the National Academy of Sciences of the United States of America, 2020. **117**(50): p. 31808-31816.
12. Devi, L., et al., *Accumulation of amyloid precursor protein in the mitochondrial import channels of human Alzheimer's disease brain is associated with mitochondrial dysfunction.* Journal of Neuroscience, 2006. **26**(35): p. 9057-9068.
13. Di Maio, R., et al., *alpha-Synuclein binds to TOM20 and inhibits mitochondrial protein import in Parkinson's disease.* Science Translational Medicine, 2016. **8**(342): p. 14.
14. Yano, H., et al., *Inhibition of mitochondrial protein import by mutant huntingtin.* Nature Neuroscience, 2014. **17**(6): p. 822-831.
15. Aguer, C., et al., *Galactose Enhances Oxidative Metabolism and Reveals Mitochondrial Dysfunction in Human Primary Muscle Cells.* Plos One, 2011. **6**(12): p. 11.
16. Eilers, M. and G. Schatz, *BINDING OF A SPECIFIC LIGAND INHIBITS IMPORT OF A PURIFIED PRECURSOR PROTEIN INTO MITOCHONDRIA.* Nature, 1986. **322**(6076): p. 228-232.
17. Rassow, J., et al., *TRANSLOCATION ARREST BY REVERSIBLE FOLDING OF A PRECURSOR PROTEIN IMPORTED INTO MITOCHONDRIA - A MEANS TO QUANTITATE TRANSLOCATION CONTACT SITES.* Journal of Cell Biology, 1989. **109**(4): p. 1421-1428.
18. Yoon, Y., K.R. Pitts, and M.A. McNiven, *Mammalian dynamin-like protein DLP1 tubulates membranes.* Molecular Biology of the Cell, 2001. **12**(9): p. 2894-2905.
19. Liesa, M., M. Palacin, and A. Zorzano, *Mitochondrial Dynamics in Mammalian Health and Disease.* Physiological Reviews, 2009. **89**(3): p. 799-845.
20. Pereira, G.C., et al., *A High-Resolution Luminescent Assay for Rapid and Continuous Monitoring of Protein Translocation across Biological Membranes.* Journal of Molecular Biology, 2019. **431**(8): p. 1689-1699.
21. Needs, H.I., et al., *The NanoLuc Assay System for Accurate Real-Time Monitoring of Mitochondrial Protein Import within Intact Mammalian Cells.* bioRxiv, 2022: p. 2022.09.23.509159.
22. Rustom, A., et al., *Nanotubular highways for intercellular organelle transport.* Science, 2004. **303**(5660): p. 1007-1010.
23. Gurke, S., J.F.V. Barroso, and H.H. Gerdes, *The art of cellular communication: tunneling nanotubes bridge the divide.* Histochemistry and Cell Biology, 2008. **129**(5): p. 539-550.
24. Gerdes, H.H., N.V. Bukoreshtliev, and J.F.V. Barroso, *Tunneling nanotubes: A new route for the exchange of components between animal cells.* Febs Letters, 2007. **581**(11): p. 2194-2201.
25. Drab, M., et al., *Inception Mechanisms of Tunneling Nanotubes.* Cells, 2019. **8**(6): p. 17.
26. Hoebeke, J., G. Vannijen, and M. Debrabander, *INTERACTION OF ONCODAZOLE (R 17934), NEW ANTI-TUMORAL DRUG, WITH RAT-BRAIN TUBULIN.* Biochemical and Biophysical Research Communications, 1976. **69**(2): p. 319-324.
27. Friedman, P.A. and E.G. Platzer, *INTERACTION OF ANTHELMINTIC BENZIMIDAZOLES AND BENZIMIDAZOLE DERIVATIVES WITH BOVINE BRAIN TUBULIN.* Biochimica Et Biophysica Acta, 1978. **544**(3): p. 605-614.
28. Debrabander, M.J., et al., *EFFECTS OF METHYL 5-(2-THIENYLCARBONYL)-1H-BENZIMIDAZOL-2-YL CARBAMATE, (R-17934-NSC-238159), A NEW SYNTHETIC ANTITUMORAL DRUG INTERFERING WITH MICROTUBULES, ON MAMMALIAN-CELLS CULTURED INVITRO.* Cancer Research, 1976. **36**(3): p. 905-916.
29. Kumar, A., et al., *Influenza virus exploits tunneling nanotubes for cell-to-cell spread.* Scientific Reports, 2017. **7**: p. 14.
30. Luchetti, F., et al., *Fas Signalling Promotes Intercellular Communication in T Cells.* Plos One, 2012. **7**(4): p. 12.
31. Cheung, T.M.J., *A small molecule dissociates the PAM motor from the TIM23 channel*, in *Biochemistry and Molecular Biology*. 2017, University of California Los Angeles. p. 123.

32. Osteikoetxea-Molnar, A., et al., *The growth determinants and transport properties of tunneling nanotube networks between B lymphocytes.* Cellular and Molecular Life Sciences, 2016. **73**(23): p. 4531-4545.
33. Miriyala, S., et al., *Novel role of 4-hydroxy-2-nonenal in AIFm2-mediated mitochondrial stress signaling.* Free Radical Biology and Medicine, 2016. **91**: p. 68-80.
34. Ohiro, Y., et al., *A novel p53-inducible apoptogenic gene, PRG3, encodes a homologue of the apoptosis-inducing factor (AIF).* Febs Letters, 2002. **524**(1-3): p. 163-171.
35. Wang, Y., et al., *Tunneling-nanotube development in astrocytes depends on p53 activation.* Cell Death and Differentiation, 2011. **18**(4): p. 732-742.
36. Vargas, J.Y., et al., *The Wnt/Ca2+ pathway is involved in interneuronal communication mediated by tunneling nanotubes.* Embo Journal, 2019. **38**(23): p. 21.
37. Hanna, S.J., et al., *The Role of Rho-GTPases and actin polymerization during Macrophage Tunneling Nanotube Biogenesis.* Scientific Reports, 2017. **7**: p. 16.
38. Zhang, S.L., M.G. Kazanietz, and M. Cooke, *Rho GTPases and the emerging role of tunneling nanotubes in physiology and disease.* American Journal of Physiology-Cell Physiology, 2020. **319**(5): p. C877-C884.
39. Wang, X. and H.H. Gerdes, *Transfer of mitochondria via tunneling nanotubes rescues apoptotic PC12 cells.* Cell Death and Differentiation, 2015. **22**(7): p. 1181-1191.
40. Zou, W.G. and D.E. Zhang, *The interferon-inducible ubiquitin-protein isopeptide ligase (E3) EFP also functions as an ISG15 E3 ligase.* Journal of Biological Chemistry, 2006. **281**(7): p. 3989-3994.
41. Yano, M., et al., *20S proteasorne prevents aggregation of heat-denatured proteins without PA700 regulatory subcomplex like a molecular chaperone.* Biomacromolecules, 2004. **5**(4): p. 1465-1469.
42. Young, J.C., N.J. Hoogenraad, and F.U. Hartl, *Molecular chaperones Hsp90 and Hsp70 deliver preproteins to the mitochondrial import receptor Tom70.* Cell, 2003. **112**(1): p. 41-50.
43. Matsumura, Y., J. Sakai, and W.R. Skach, *Endoplasmic Reticulum Protein Quality Control Is Determined by Cooperative Interactions between Hsp/c70 Protein and the CHIP E3 Ligase.* Journal of Biological Chemistry, 2013. **288**(43): p. 31069-31079.
44. Pepe, A., et al., *Tunneling nanotubes provide a route for SARS-CoV-2 spreading.* Science Advances, 2022. **8**(29): p. 17.
45. Jackson, M.V., et al., *Mitochondrial Transfer via Tunneling Nanotubes is an Important Mechanism by Which Mesenchymal Stem Cells Enhance Macrophage Phagocytosis in the In Vitro and In Vivo Models of ARDS.* Stem Cells, 2016. **34**(8): p. 2210-2223.
46. Chinnery, H.R. and K.E. Keller, *Tunneling Nanotubes and the Eye: Intercellular Communication and Implications for Ocular Health and Disease.* Biomed Research International, 2020. **2020**: p. 15.
47. Dupont, M., et al., *Tunneling nanotubes: intimate Communication between Myeloid Cells.* Frontiers in Immunology, 2018. **9**: p. 6.
48. Souriant, S., et al., *Tuberculosis Exacerbates HIV-1 Infection through IL-10/STAT3-Dependent Tunneling Nanotube Formation in Macrophages.* Cell Reports, 2019. **26**(13): p. 3586-+.
49. Eugenin, E.A., P.J. Gaskill, and J.W. Berman, *Tunneling nanotubes (TNT) are induced by HIV-infection of macrophages: A potential mechanism for intercellular HIV trafficking.* Cellular Immunology, 2009. **254**(2): p. 142-148.
50. Scheiblich, H., et al., *Microglia jointly degrade fibrillar alpha-synuclein cargo by distribution through tunneling nanotubes.* Cell, 2021. **184**(20): p. 5089-+.
51. Zhang, K.J., et al., *Intercellular transport of Tau protein and beta-amyloid mediated by tunneling nanotubes.* American Journal of Translational Research, 2021. **13**(11): p. 12509-12522.
52. Yablonska, S., et al., *Mutant huntingtin disrupts mitochondrial proteostasis by interacting with TIM23.* Proceedings of the National Academy of Sciences of the United States of America, 2019. **116**(33): p. 16593-16602.

53. Needs, H.I., J.M. Henley, and I. Collinson, *Perturbation of the mitochondrial import machinery by disease prone Tau affects organelle morphology and reduces neuronal complexity.* bioRxiv, 2022: p. 2022.11.30.518502.
54. Tardivel, M., et al., *Tunneling nanotube (TNT)-mediated neuron-to neuron transfer of pathological Tau protein assemblies.* Acta Neuropathologica Communications, 2016. **4**.
55. Abounit, S., et al., *Tunneling nanotubes: A possible highway in the spreading of tau and other prion-like proteins in neurodegenerative diseases.* Prion, 2016. **10**(5): p. 344-351.
56. Valdinocci, D., et al., *Alpha-Synuclein Aggregates Associated with Mitochondria in Tunnelling Nanotubes.* Neurotoxicity Research, 2021. **39**(2): p. 429-443.
57. Gousset, K., et al., *Prions hijack tunnelling nanotubes for intercellular spread.* Nature Cell Biology, 2009. **11**(3): p. 328-U232.
58. Sowinski, S., et al., *Membrane nanotubes physically connect T cells over long distances presenting a novel route for HIV-1 transmission.* Nature Cell Biology, 2008. **10**(2): p. 211-219.
59. Zhao, F.J. and M.H. Zou, *Role of the Mitochondrial Protein Import Machinery and Protein Processing in Heart Disease.* Frontiers in Cardiovascular Medicine, 2021. **8**: p. 21.
60. Palmer, C.S., A.J. Anderson, and D. Stojanovski, *Mitochondrial protein import dysfunction: mitochondrial disease, neurodegenerative disease and cancer.* Febs Letters, 2021. **595**(8): p. 1107-1131.
61. Lei, X.H. and B.R. Bochner, *Optimization of cell permeabilization in electron flow based mitochondrial function assays.* Free Radical Biology and Medicine, 2021. **177**: p. 48-57.
62. Abounit, S., E. Delage, and C. Zurzolo, *Identification and Characterization of Tunneling Nanotubes for Intercellular Trafficking.* Current Protocols in Cell Biology, 2015. **67**(1): p. 12.10.1-12.10.21.
63. Rueden, C.T., et al., *ImageJ2: ImageJ for the next generation of scientific image data.* Bmc Bioinformatics, 2017. **18**: p. 26.
64. Schindelin, J., et al., *Fiji: an open-source platform for biological-image analysis.* Nature Methods, 2012. **9**(7): p. 676-682.
65. Cross, S. *miaanalysis/mia: Version 0.21.0*. 2021 [cited 2022 18th January].
66. Seager, R.A., *Investigating the role of SUMOylation of Mitochondrial Fission Factor in Mitochondrial Dynamics*. 2020, University of Bristol. p. 289.
67. Cross, S. and R. Seager. *Colocalisation analysis macros and workflows*. 2022.
68. Valente, A.J., et al., *A simple ImageJ macro tool for analyzing mitochondrial network morphology in mammalian cell culture.* Acta Histochemica, 2017. **119**(3): p. 315-326.

Acknowledgments:
We gratefully acknowledge access and support of the Wolfson Bioimaging Facility for imaging support. We are grateful to Dr Stephen Cross and Dr Richard Seager for image analysis support. We gratefully acknowledge the University of Bristol Proteomics Facility, specifically Dr Kate Heesom, for support with TMT-MS, and Dr Phil Lewis for bioinformatics support.

Funding:
This work was funded by the Welcome Trust: through the Wellcome Trust *Dynamic Molecular Cell Biology* PhD programme (HIN, 083474; EG, 218510) and a Wellcome Investigator award (IC and GCP, 104632).

The funders had no role in study design, data collection and interpretation, or the decision to submit the work for publication. For the purpose of Open Access, the authors have applied a CC BY public copyright license to any Author Accepted Manuscript version arising from this submission.

Author contributions:
HIN, EG, GCP, MPD, JMH and IC designed experiments; HIN, EG, AW and WH conducted experiments; HIN, GCP, JMH and IC wrote the manuscript; IC and JMH secured funding and led the project.

Competing interests:

The authors declare no competing interests.

Data and materials availability:

All data are available in the main text or the supplementary materials.

Supplementary Materials contains:

Materials and Methods

Figs. S1-S14

Table S1

Caption for Movie S1

References (*61–68*)

Movie S1 (included as a separate downloadable file)

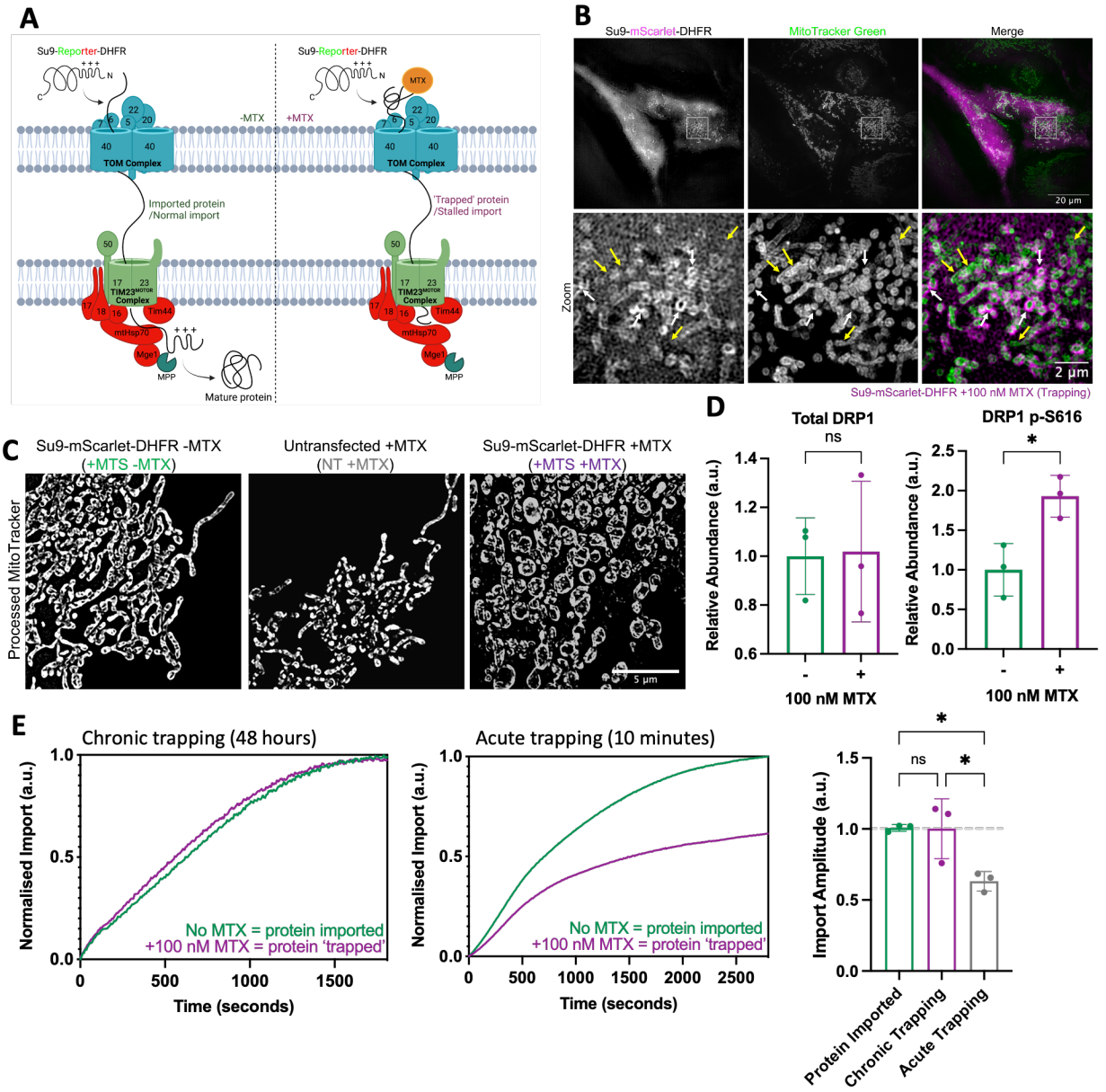

Fig. 1. Chronic precursor trapping induces mitochondrial fission but has no impact on import. **(A)** In the absence of MTX (*left*), the precursor protein (*Su9-Reporter-DHFR*) is imported into mitochondria *via* the presequence pathway. In the mitochondrial matrix, the MTS is cleaved by MPP, and it folds to form the mature protein. In the presence of MTX (*right*), MTX binds to DHFR in the cytosol, preventing it from unfolding, and thus preventing it from crossing the TOM40 channel. Since the protein contains a long Su9-Reporter region before the DHFR, this region forms a plug through the TOM40 and TIM23 channels, mimicking a stalled or aggregated precursor protein within the presequence pathway. *Schematic created using BioRender.*

(B) Representative SR 3D-SIM images showing trapping substrate accumulation around mitochondrial membranes in HeLaGAL cells expressing *Su9-mScarlet-DHFR* (magenta; 48h) in the presence of 100 nM MTX. Mitochondria are shown by MitoTracker Green staining (green). White arrows show association of trapping construct with mitochondria, yellow arrows show mitochondria not surrounded by precursor. Images are representative of N=3 biological replicates.

(C) Representative SR 3D-SIM images showing mitochondrial morphology of HeLaGAL cells subjected to trapping (+MTS +MTX) or not (+MTS -MTS). Untransfected cells in the same well as cells subjected to trapping were used as an internal control for MTX treatment (NT +MTX). Images are representative of N=3 biological replicates. Unprocessed and uncropped images are shown in supplementary Fig. S5, quantified in S6.

(D) Quantification of Western blots showing abundance of total DRP1 (*left*) or phospho-DRP1 S616 (*right*) in whole cell lysates from HeLaGAL cells expressing *Su9-EGFP-DHFR* in the absence or presence of 100 nM MTX. Normalised to β-actin loading control and -MTX control. N=3 biological replicates. Error bars represent SD. Representative blots are shown in supplementary Fig. S7.

(E) NanoLuc import traces after precursor trapping. For chronic trapping (*left panel*), *Cox8a-11S* expressing HeLaGAL cells were subjected to expression of *Su9-mScarlet-DHFR* in the presence (purple; trapped precursor) or absence (green; imported precursor) of 100 nM MTX for 48 hours. For acute trapping (*middle panel*), HeLaGAL cells expressing *Cox8a-11S* were permeabilised using 3 nM rPFO prior to incubation (RT, 10 min) with 1 μM trap substrate (*Su9-ACP1-DHFR*), in the presence (purple; trapped precursor) or absence (green; imported precursor) of 100 nM MTX. NanoLuc import assays were then carried out to monitor import of precursor protein *Su9-EGFP-pep86*. Traces were normalised to eqFP670 fluorescence (as a marker of *Cox8a-11S* expression levels), technical replicates averaged, then normalised to the maximum value for the given run, and finally normalised to the +/- MTX (-MTS) control. Maximum import (amplitude) is shown (right panel). One-way ANOVA and Tukey's *post-hoc* test were used to determine significance. Error bars represent SD. N=3 biological replicates, each with n=3 technical replicates.

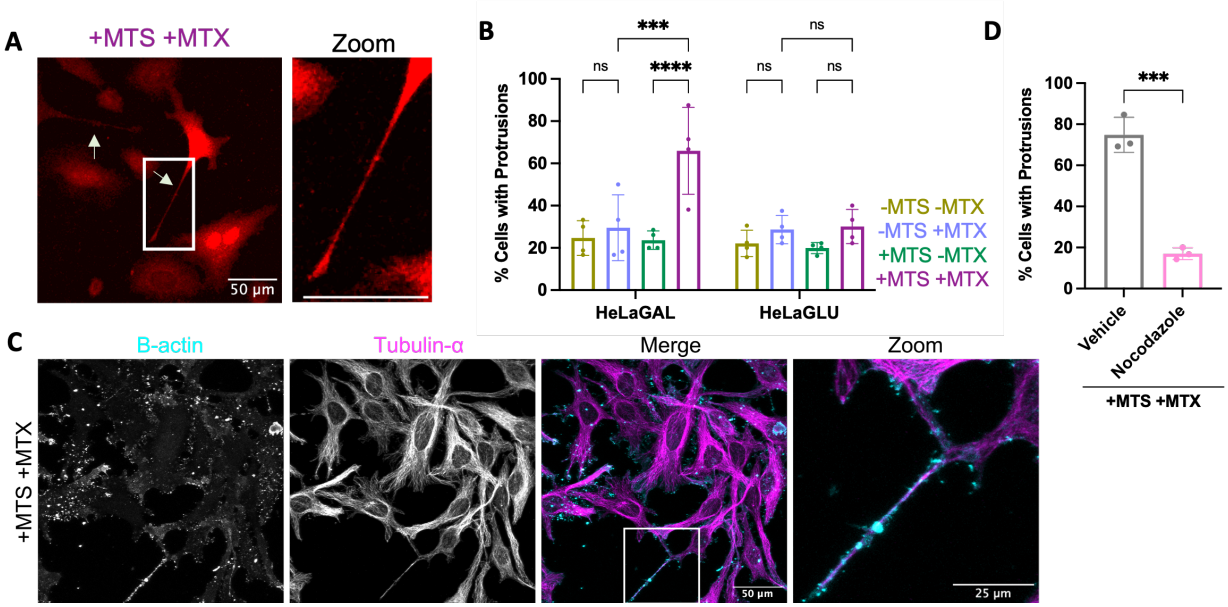

Fig. 2. Chronic precursor trapping induces formation of TNTs.
(A) Representative confocal images showing cell morphology of HeLaGAL cells subjected to expression of *mCherry* (red) and *Su9-EGFP-DHFR* in the presence of 100 nM MTX (+MTS +MTX; trapped precursor). Arrows indicate protrusions, and box highlights zoom region. N=4 biological replicates.
(B) Quantification of the proportion of transfected cells with protrusions. All representative images shown in supplementary Fig. S8. Error bars show SD. Two-way ANOVA and Tukey's *post-hoc* test were used to determine significance. N=4 biological replicates; 20 cells counted per replicate.
(C) Representative confocal images showing tubulin and actin staining of protrusions. HeLaGAL cells were subjected to trapping for 48 h to induce protrusion formation. Cells were fixed and stained with antibodies against β-actin (Sigma; A2228) and tubulin-α (BioRad; MCA78G) and visualised by confocal microscopy to observe protrusion composition. N=4 biological replicates.
(D) Quantification of the proportion of HeLaGAL cells, subjected to precursor trapping, with protrusions following treatment for 48 hours in the absence (vehicle; DMSO only) or presence of 100 nM nocodazole. Cells were pre-treated with 100 nM MTX for 16 h, then treated with nocodazole at the same time as transduction with the trapping precursor and incubated for 48 h prior to imaging. Representative confocal images shown in supplementary Fig. S9. Error bars show SD. Unpaired t-test was used to determine difference between groups. N=3 biological replicates; 20 cells counted per replicate.

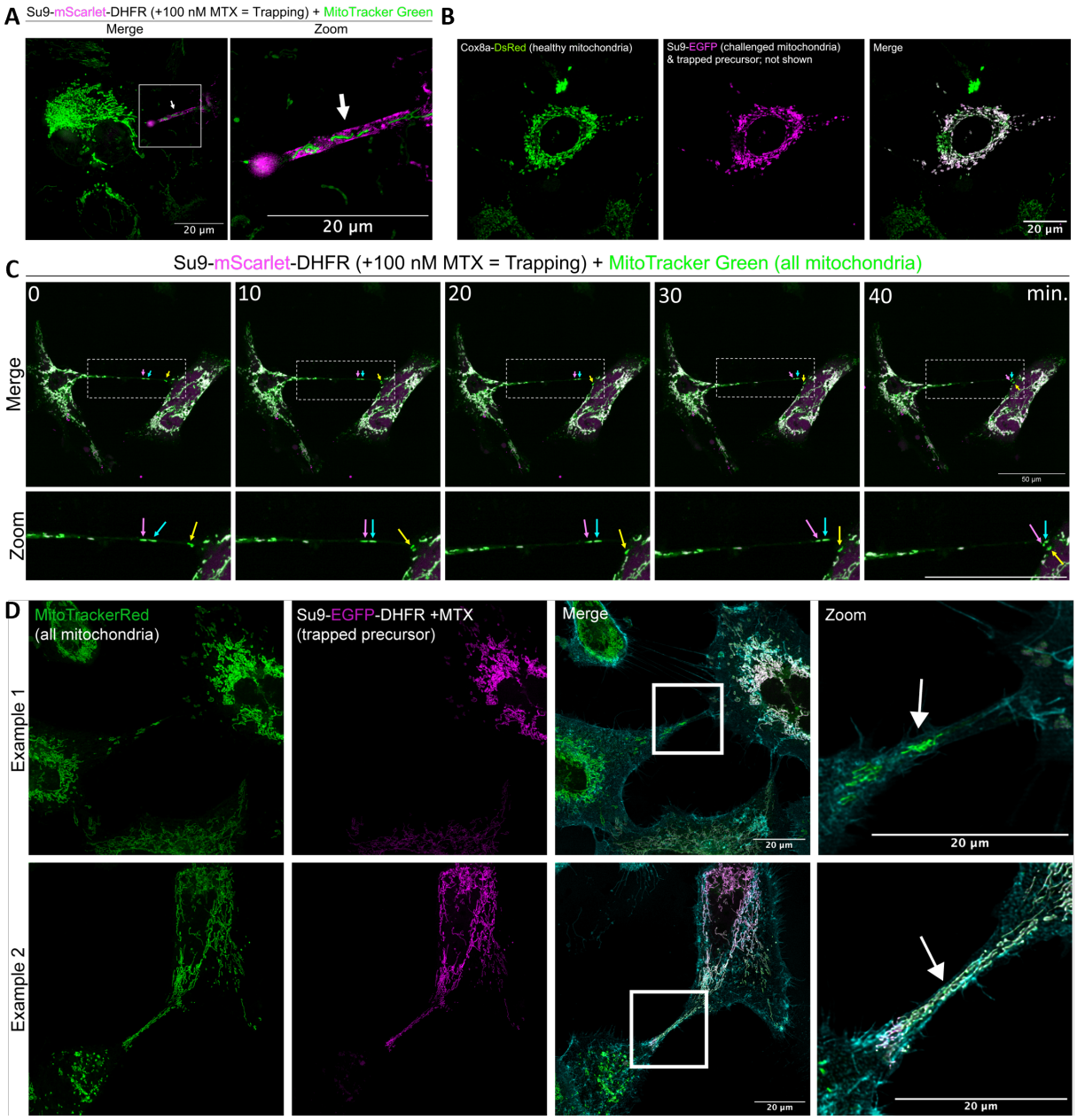

Fig. 3. Chronic precursor trapping induces intercellular mitochondrial transfer *via* TNTs.
(A) Representative SR 3D-SIM image showing mitochondria (MitoTracker Green; green) within a TNT formed between a HeLaGAL cell with trapped precursor (*Su9-mScarlet-DHFR*; magenta), and an untransfected neighbour (green mitochondria, unlabeled cytosol). Cells were pre-treated for 16 h with 100 nM MTX, transfected with *Su9-mScarlet-DHFR* and incubated for 48 hours prior to mitochondrial staining with MitoTracker Green and live imaging by SIM. Arrow highlights TNT and box indicates zoom area. N=3 biological replicates.
(B) Representative confocal images from co-culture experiments, showing mitochondrial transfer between healthy and sick cells. Mitochondria of one batch of HeLaGAL cells were subjected to *Cox8a-dsRed* overexpression (healthy mitochondria; green). A second batch of cells was subjected to *Su9-EGFP* expression (magenta) and sequential trapping (*Su9-eqFP670-DHFR* +100 nM MTX). After 48 hours, cells were washed, detached, counted, and mixed at equal ratios, prior to reseeding on coverslips. Cells were co-

cultured for a further 8 hours before fixation and visualisation by confocal microscopy. N=3 biological replicates.

(C) Time series of still images from a representative time-lapse movie showing the transfer of healthy mitochondria (MitoTracker Green; green) within a TNT into a cell with trapped precursor (*Su9-mScarlet-DHFR* (magenta) +100 nM MTX). Cells were imaged live using an Olympus IXplore SpinSR system. Each timeframe is a Max z-projection of 10 slices, taken every 5 min x 10 timepoints. Full movie shown in supplementary Movie S1.

(D) Representative confocal images showing mitochondria (MitoTracker Red; green) within a TNT (plasma membrane stained with Wheat Germ Agglutinin (WGA); cyan) formed between a HeLaGAL cell with trapped precursor (*Su9-EGFP-DHFR*; magenta), and an untransfected healthy neighbour (green mitochondria). Example 1 shows healthy mitochondria being transferred to an unhealthy cell; example 2 shows unhealthy mitochondria being transferred to a healthy cell. Cells were transfected with *Su9-EGFP-DHFR* and incubated for 48 hours in the presence of 100 nM MTX prior to staining with MitoTracker Red and WGA. Cells were then fixed and imaged. Box indicates zoom area and arrow highlights TNT. N=3 biological replicates.

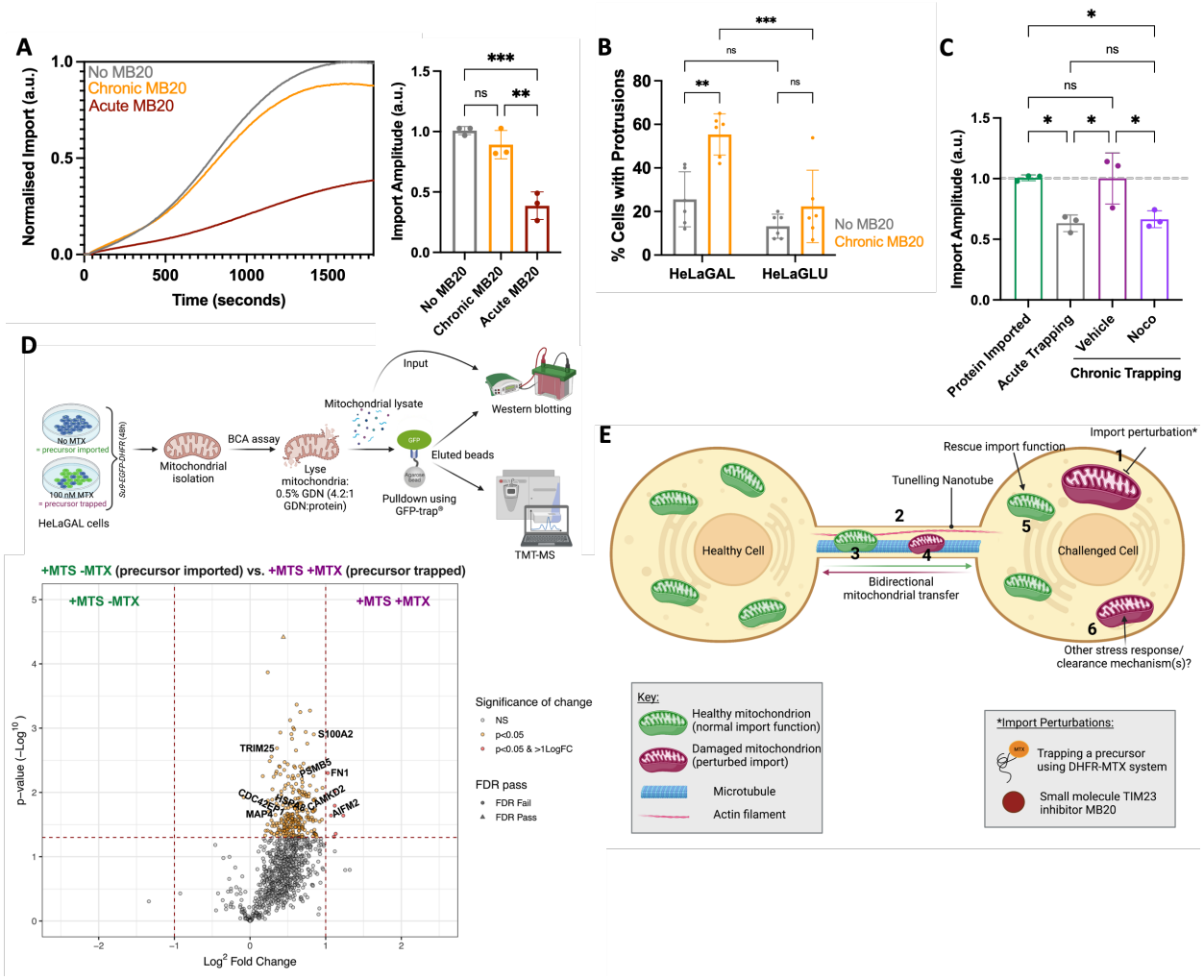

Fig. 4. Intercellular mitochondrial transfer *via* TNTs rescues import function.

(A) NanoLuc import traces showing precursor protein (*Su9-EGFP-pep86*) import in *Cox8a-11S* expressing HeLaGAL cells treated with vehicle only (DMSO; no MB20; grey), or with either chronic (48 h; orange) or acute (10 min; red) MB20 exposure. Quantification of import amplitude is shown in right hand panel. N=3 biological replicates, each with 3 technical replicates. Error bars represent SD. One-way ANOVA with Tukey's *post-hoc* test was used to determine significance.

(B) Quantification of proportion of cells with TNTs following chronic treatment with 10 µM MB20 (48 h). Representative confocal images shown in supplementary Fig. S10. N=6 biological replicates; 20 cells counted per replicate. Error bars represent SD. Two-way ANOVA and Tukey's *post-hoc* test were used to determine significance.

(C) Quantification of import amplitude in cells subjected to trapping, in response to treatment with nocodazole. HeLaGAL cells expressing *Cox8a-11S* were subjected to trapping (+MTX) or not (-MTX) and treated with 100 nM nocodazole (*noco*), or DMSO only (*vehicle*) for 48 hours prior to monitoring the import of *Su9-EGFP-pep86* by NanoLuc import assays. Import trace is shown in supplementary Fig. S12. N=3 biological replicates, each with 3 technical replicates. Error bars represent SD. One-way ANOVA with Tukey's *post-hoc* test was used to determine significance.

(D) HeLaGAL cells were subjected to *Su9-EGFP-DHFR* expression in the presence or absence of 100 nM MTX for 48 h. Mitochondria were isolated and mitochondrial protein content was assessed using a BCA assay. Equal amounts of mitochondria were lysed using 0.5% GDN at a ratio of 4.2:1 (GDN: protein). A fraction of mitochondrial lysate was saved as an input control, and the rest was loaded onto GFP-trap agarose beads, to pull-down proteins associated with the GFP tagged protein of interest (trapped or imported

precursor). The resulting beads conjugated to proteins associated with GFP-tagged proteins were analysed by Western blot and TMT-MS. Lower panel shows a volcano plot highlighting proteins enhanced in pulldown samples from mitochondria with imported precursor (+MTS -MTX, *left*) compared to those with the trapped precursor (+MTS +MTX, *right*). Selected proteins of interest are highlighted by gene names on the volcano plot and the full list is provided in supplementary Table S1. A representative Western blot is shown in supplementary Fig. S13 and control (-MTS, +/- MTX) volcano plot in supplementary Fig. S14. N=3 biological replicates. *Top panel schematic created using BioRender.*

(E) Proposed import rescue mechanism *via* TNT-dependent intercellular mitochondrial transfer. Cells subjected to import perturbations *(1)* induce the formation of TNTs composed of microtubules and actin filaments *(2).* TNTs allow transfer of healthy mitochondria from neighboring cells into cells with challenged mitochondria *(3),* whilst also allowing clearance of damaged mitochondria to neighboring healthy cells *(4)*. The transfer and integration of healthy mitochondria with normal import function, and disposal of mitochondria with defective import, rescues the overall cellular import function *(5)*. This rescue effect is likely enhanced by additional stress response mechanisms *(6). Schematic created using BioRender.*

Supplementary Materials for

Intercellular Mitochondrial Transfer as a Rescue Mechanism in Response to Protein Import Failure

Hope I Needs[1], Gonçalo C. Pereira[1*], Emily Glover[1], Alina Witt[2], Wolfgang Hübner[2], Mark P. Dodding[1], Jeremy M Henley[1,†] and Ian Collinson[1,†]

Affiliations:

[1] *School of Biochemistry, University of Bristol, Bristol BS8 1TD, UK*

[2] *Fakultät für Physik, Universität Bielefeld, Postfach 100131 D-33501, Germany*

[†], corresponding authors: ian.collinson@bristol.ac.uk and J.M.Henley@bristol.ac.uk

[*], present address: *MRC - Mitochondrial Biology Unit, University of Cambridge, The Keith Peters Building, Cambridge Biomedical Campus, Cambridge CB2 0XY, UK*

This PDF file includes:

Materials and Methods
Figs. S1 to S14
Table S1
Caption for Movie S1

Other Supplementary Materials for this manuscript include the following:

Movie S1

Materials and Methods

Reagents

All chemicals were of the highest grade of purity commercially available and purchased from Sigma, UK, unless stated otherwise. Aqueous solutions were prepared in ultrapure water, while for non-aqueous solutions, ethanol or DMSO was used as solvent instead. Antibody catalogue numbers and suppliers are detailed in figure legends.

Generation of Constructs

Constructs were generated by standard cloning techniques. Briefly, PCR reactions were carried out using Q5 High Fidelity Hot Start DNA Polymerase (New England Biolabs (NEB)), using 20 pmol primers and 200 pg template DNA, as per manufacturers' instructions. PCR products were purified using QIAquick PCR Purification Kit (QIAgen). Restriction digest reactions were carried out using NEB restriction enzymes at 37ºC for 45 min. Ligation reactions were carried out using T4 DNA Ligase (NEB) overnight at 16ºC. Transformation was carried out in *E. coli* cells (α-select, XL1-Blue, or BL21-DE3 cells were used, depending on application; all originally sourced from NEB) for 30 min on ice, followed by heat shocking (45 sec, 42ºC), and a further 15 min on ice. Cells were recovered by incubating in LB media at 37ºC for 1 h and then plated on LB-agar plates containing appropriate antibiotic. Plasmids were prepared by mini or maxi preps using commercially available kits (Qiagen and Promega, respectively) following manufacturers' instructions, and verified by DNA sequencing using Eurofins Genomics TubeSeq service.

Protein Purification

Protein expression was carried out exactly as described previously [20]. A single colony of transformed BL21 (DE3) bacteria was grown as a pre-culture in LB with appropriate antibiotic overnight (37°C; 200 rpm). Pre-cultures were used to inoculate a secondary culture at a 1:100 dilution, in 2X YT supplemented with appropriate antibiotic. Secondary cultures were grown until mid-log phase, then induced with 1 mM IPTG or 0.2% (w/v) Arabinose and grown for a further 3 h. Cells were harvested by centrifugation (15 min; 6000 xg), resuspended in TK buffer (20 mM TRIS base, 50 mM KCl; pH 8.0), cracked in a cell disruptor (Constant Systems; 2 cycles at 25 kpsi), and clarified by centrifugation (45 min; 38,000 rpm).

GST tagged Recombinant Perfringolysin (rPFO)

Supernatant (soluble fraction) was loaded onto a 5 mL GSTrap 4B column (GE Healthcare) and the column was washed with TK buffer until the absorbance of the flow through ceased to decrease any further. The peptide was eluted using 10 μM reduced glutathione, prepared fresh. Eluted fractions were pooled and

loaded onto a 5 mL anionic exchanger (Q- column; GE Healthcare). A salt gradient of 0-1 M was applied over 20 min and the protein was eluted in 5 mL fractions. The fractions containing the protein were confirmed by SDS-PAGE with Coomassie staining, then pooled and spin concentrated. The final protein concentration was determined based on an extinction coefficient of 117,120 M^{-1} cm^{-1}. The protein was aliquoted, snap frozen, and stored at -80ºC until required. For each assay, a fresh aliquot was thawed, used immediately, and discarded afterwards, due to the instability of this protein [61].

GST-Dark Peptide

GST-Dark was prepared as described previously [20]. Supernatant was loaded onto a GSTrap 4B column and purification was carried out exactly as for rPFO but without the ion exchange chromatography. Analysis, yield, and freezing was carried out exactly as for rPFO. Protein concentration was determined based on an extinction coefficient of 48,360 M^{-1} cm^{-1}.

His tagged Su9-EGFP-pep86

Inclusion bodies (insoluble fraction) were solubilised in TK buffer supplemented with 6 M urea, before loading onto a 5 mL HisTrap HP column (GE Healthcare). The protein was eluted in 300 mM imidazole. Eluted fractions containing the desired protein were pooled and loaded onto a 5 mL cationic exchanger (S-column; GE Healthcare). A salt gradient of 0-1 M was applied over 20 min and the protein was eluted in 5 mL fractions. Imidazole was removed by spin concentration, followed by dilution in TK buffer containing 6 M urea. Analysis, yield, and freezing were carried out exactly as for rPFO. Protein concentration was determined based on an extinction coefficient of 28,880 M^{-1} cm^{-1}.

His-SUMO--Su9-ACP1-D-ACP1-D-DHFR-Myc

His-SUMO--Su9-ACP1-D-ACP1-D-DHFR-Myc was produced as described previously [3]. It was expressed by induction with IPTG, and cells were grown for a further 18 hours prior to harvesting. Subsequently, proteins from the soluble fraction were purified using a Nickel column, and finally contaminants were removed by size exclusion chromatography using a HiLoad 16/60 Superdex gel filtration column (Cytiva, UK). The SUMO tag was cleaved from the protein using Ulp1 protease following purification, and the eluted sample passed through a Nickel column to separate the SUMO-His tag from the protein. Protein concentration was determined based on an extinction coefficient of 42,400 M^{-1} cm^{-1}.

Cell Culture

HEK293T (ECACC) and glucose-grown HeLa cells (HeLaGLU; ATCC) were maintained in Dulbecco's Modified Eagle's Medium (DMEM; Gibco; 41965039) supplemented with 10% (v/v) foetal bovine calf serum (FBS; Invitrogen) and 1% (v/v) penicillin-streptomycin (P/S; Invitrogen). When OXPHOS dependence was required, HeLa cells were cultured in galactose medium (HeLaGAL; ATCC) consisting of DMEM without glucose (Gibco; 11966025) supplemented with 10 mM galactose, 1 mM sodium pyruvate, 10% FBS and 1% P/S. Cells were cultured in galactose media for at least 3 weeks prior to experiments on HeLaGAL cells. Cells were maintained in T75 ventilated flasks in humidified incubators at 37ºC with 5% CO_2.

Cell Transduction by Transfection

HeLa cells were plated and grown up to ~70-80% confluency. At this point cells were transfected with 1 µg (per 35mm dish) of the desired DNA using Lipofectamine 3000 reagent (Thermo Fisher Scientific), at a 1:1.5 ratio of DNA:Lipofectamine, following the manufacturers' protocol. Cells were then grown for a further 24-72 h prior to experimental analysis.

Cell Transduction by Lentiviral Infection

Lentiviral particles were produced in HEK293T cells by addition of a mixture of DNAs (27.2 µg DNA to be produced, and packaging vectors pMDG2 (6.8 µg) and pAX2 (20.4 µg)) and 1 µg/µL pEI transfection reagent in OptiMEM media (Gibco) to HEK293T cells in a T75 flask, followed by incubation for 6 hours at 37ºC, 5% CO_2. Media was then changed to complete DMEM, and cells incubated for 72 h to allow lentivirus particle production. Lentiviral particles were harvested at 48 and 72 h for maximum yield, pooled, spun down at 4000 xg for 5 min to remove dead cells, and concentrated by adding Lenti-X concentrator (Takara Bio) at a 1:3 ratio and incubating at 4ºC for at least 1 h. Lentivirus was then pelleted by centrifugation at 4000 xg for 45 min. Pellets were resuspended in plain DMEM at 1:50 of initial supernatant volume and aliquoted and stored at -80ºC until required. For infection, concentrated lentivirus (volume optimised by titration of each fresh batch) was added dropwise to cell media when cells were at ~70-80% confluency and incubated for 24-72 h prior to experimental analysis.

Total Protein Cell Lysis

For extraction of total protein lysate, cells were washed extensively with HBSS, and RIPA buffer (Sigma, supplemented with 1 mM PMSF) was added (200 µL for ~35 mm surface, scaled up or down appropriately). Cells were scraped on ice into Eppendorf tubes, which were incubated for 1 h on a rotating wheel at 4ºC, prior to spinning down at 10,000 xg for 15 min at 4ºC. Supernatant (containing proteins) was stored at -

20ºC. If protein concentration was required, this was obtained by carrying out a BCA assay (Pierce™ BCA Protein Assay Kit, Thermo Fisher Scientific), following manufacturer's instructions and using BSA as a standard.

Western Blotting

Following total protein extraction, protein samples were heated to 95ºC for 5 min in the presence of LDS supplemented with 50 mM DTT. 30 µg of total protein was loaded on 4-12% BOLT gels (Thermo Fisher Scientific), separated (200 V, 24 min), and transferred onto polyvinylidene difluoride (PVDF) membranes (activated with methanol; Thermo Fisher Scientific) with transfer buffer (336 mM tris, 260 mM glycine, 140 mM tricine, 2.5 mM EDTA) using a semi-dry Pierce Power Station transfer system (Thermo Fisher Scientific; 25 V, 2.5 mAmp, 10 min). Membranes were blocked for 1 h in milk or BSA (5% w/v in TBS-T: 20 mM TRIS, 1.5 M NaCl, 0.1% (v/v) Tween-20 (pH 7.6)) and incubated in 5% milk or BSA containing the appropriate primary antibody (see figure legends; 4°C, overnight). Membranes were washed extensively with TBS-T and probed with appropriate secondary antibody in 2.5% milk or BSA (RT, 1 hour). Membranes were washed with TBS-T, incubated with ECL substrate (GE Healthcare), and developed using an Odyssey Fc Imaging System (LI-COR). Analysis and quantification were carried out using Image Studio Lite software

Mitochondrial Isolation

Confluent cells were harvested by trypsinisation, pelleted, and washed extensively with HBSS. Pellets were frozen overnight at -80ºC and thawed the next day, to weaken membranes. Subsequently, mitochondrial isolation was performed using Mitochondrial Isolation Kit for Cultured Cells (Abcam; ab110170) following manufacturers' instructions. Mitochondrial protein concentration was calculated by BCA assay.

Immunoprecipitation

Following mitochondrial isolation, mitochondria were gently lysed using 4.2g/g GDN (4.2g GDN: 1g protein) in IP buffer (0.1 M TRIS-HCl, 0.15 M NaCl, phospholipids (0.03mg/ml PE; 0.03mg/ml PG; 0.09mg/ml PC), 1X cOmplete ULTRA Protease Inhibitor Cocktail). GFP-tagged proteins were isolated using 10 µL GFP-trap beads (Chromotek). Supernatant (lysed mitochondrial sample) was incubated on a rotating wheel with beads overnight at 4ºC. Subsequently, beads were washed in IP buffer. After washing, supernatant was removed, and samples were analysed by Western blotting or mass spectrometry.

Proteomic analysis

TMT Labelling and High pH reversed-phase chromatography

Immuno-isolated samples were reduced (10 mM TCEP, 55°C for 1 h), alkylated (18.75 mM iodoacetamide, room temperature for 30 min) and then digested from the beads with trypsin (2.5 µg trypsin; 37°C, overnight). The resulting peptides were then labeled with TMTpro sixteen-plex reagents according to the manufacturer's protocol (Thermo) and the labelled samples pooled and desalted using a SepPak cartridge, according to the manufacturer's instructions (Waters). Eluate from the SepPak cartridge was evaporated to dryness and resuspended in buffer A (20 mM ammonium hydroxide, pH 10) prior to fractionation by high pH reversed-phase chromatography using an Ultimate 3000 liquid chromatography system (Thermo). In brief, the sample was loaded onto an XBridge BEH C18 Column (130Å, 3.5 µm, 2.1 mm X 150 mm, Waters) in buffer A and peptides eluted with an increasing gradient of buffer B (20 mM Ammonium Hydroxide in acetonitrile, pH 10) from 0-95% over 60 min. The resulting fractions (6 in total) were evaporated to dryness and resuspended in 1% formic acid prior to analysis by nano-LC MSMS using an Orbitrap Fusion Lumos mass spectrometer (Thermo).

Nano-LC Mass Spectrometry

High pH RP fractions were further fractionated using an Ultimate 3000 nano-LC system in line with an Orbitrap Fusion Lumos mass spectrometer (Thermo). In brief, peptides in 1% (vol/vol) formic acid were injected onto an Acclaim PepMap C18 nano-trap column (Thermo). After washing with 0.5% (v/v) acetonitrile 0.1% (v/v) formic acid peptides were resolved on a 250 mm × 75 µm Acclaim PepMap C18 reverse phase analytical column (Thermo) over a 150 min organic gradient, using 7 gradient segments (1-6% solvent B over 1 min, 6-15% B over 58 min, 15-32% B over 58 min, 32-40% B over 5 min, 40-90% B over 1 min, held at 90% B for 6 min and then reduced to 1% B over 1 min) with a flow rate of 300 nl min^{-1}. Solvent A was 0.1% formic acid and Solvent B was aqueous 80% acetonitrile in 0.1% formic acid. Peptides were ionized by nano-electrospray ionization at 2.0kV using a stainless-steel emitter with an internal diameter of 30 µm (Thermo) and a capillary temperature of 300°C.

All spectra were acquired using an Orbitrap Fusion Lumos mass spectrometer controlled by Xcalibur 3.0 software (Thermo) and operated in data-dependent acquisition mode using an SPS-MS3 workflow. FTMS1 spectra were collected at a resolution of 120 000, with an automatic gain control (AGC) target of 200 000 and a max injection time of 50 ms. Precursors were filtered with an intensity threshold of 5000, according to charge state (to include charge states 2-7) and with monoisotopic peak determination set to Peptide. Previously interrogated precursors were excluded using a dynamic window (60 s +/-10 ppm). The MS2 precursors were isolated with a quadrupole isolation window of 0.7 m/z. ITMS2 spectra were collected with an AGC target of 10 000, max injection time of 70 ms and CID collision energy of 35%.

For FTMS3 analysis, the Orbitrap was operated at 50 000 resolution with an AGC target of 50 000 and a max injection time of 105 ms. Precursors were fragmented by high energy collision dissociation (HCD) at a normalised collision energy of 60% to ensure maximal TMT reporter ion yield. Synchronous Precursor Selection (SPS) was enabled to include up to 10 MS2 fragment ions in the FTMS3 scan.

Data Analysis

The raw data files were processed and quantified using Proteome Discoverer software v2.4 (Thermo) and searched against the UniProt Human database (downloaded January 2021: 169297 entries) using the SEQUEST HT algorithm. Peptide precursor mass tolerance was set at 10 ppm, and MS/MS tolerance was set at 0.6 Da. Search criteria included oxidation of methionine (+15.995 Da), acetylation of the protein N-terminus (+42.011 Da) and Methionine loss plus acetylation of the protein N-terminus (-89.03 Da) as variable modifications and carbamidomethylation of cysteine (+57.0214) and the addition of the TMTpro mass tag (+304.207) to peptide N-termini and lysine as fixed modifications. Searches were performed with full tryptic digestion and a maximum of 2 missed cleavages were allowed. The reverse database search option was enabled and all data was filtered to satisfy false discovery rate (FDR) of 5%.

Light Microscopy Analysis

Fixed Cell Confocal Microscopy

For staining with dyes, cells on glass coverslips were incubated with 100 nM MitoTrackerRed CMXRos (Invitrogen) for 30 min at 37ºC then washed twice in HBSS. Cells were then incubated with 5 µg/mL Wheat Germ Agglutin (WGA) Alexa Fluor 633 (Thermo) for 10 min at RT then washed three times in HBSS followed by fixation (protocol adapted from [62]). Coverslips were washed three times in HBSS then incubated in fixative 1 (2% (w/v) paraformaldehyde (PFA), 0.05% (w/v) glutaraldehyde, 0.2 M HEPES in PBS) for 20 min at RT. Fixative 1 was removed and coverslips were incubated with fixative 2 (4% (w/v) PFA, 0.2 M HEPES in PBS) for a further 20 min at RT. Coverslips were washed once with 100 mM glycine in PBS for 4 min followed by three quick washes in PBS. Coverslips were dipped in ddH_2O before mounting using Fluoromount-G mounting medium (Thermo). Cells were imaged using a Leica confocal microscope (SP8) with 'lightning' adaptive image restoration, and Leica Application Suite X (LAS X) software platform. Laser lines used were 488, 562, and 633 nm, with gain set to allow maximum sensitivity without saturation, and z-stacks were taken.

For immunocytochemistry, following fixation and quenching (as above), cells were permeabilised by incubation in 0.1% (v/v) Triton-X in PBS for 5 min, washed in PBS and blocked with 3% (w/v) BSA in PBS for 30 min. Coverslips were incubated on a drop of primary antibody in 3% BSA overnight at 4ºC.

Coverslips were washed extensively in PBS and incubated with the appropriate secondary antibody (2 h, RT) in 3% BSA, then washed again. Coverslips were dipped in ddH2O and mounted using Fluoromount-G. Coverslips were left to dry overnight and imaged using a Leica confocal microscope (SP5II or SP8) and LAS X software platform. Laser lines used were 405, 488, 562, and 633 nm, with gain set to allow maximum sensitivity without saturation, and z-stacks were taken.

Live Cell Confocal Microscopy

Cells were seeded onto 35 mm glass bottomed dishes (Corning). Immediately prior to imaging, cells were washed in HBSS, transferred to imaging media (10% FBS, 2 mM L-Glutamine, 10 mM D-Galactose, 1 mM Sodium Pyruvate, 40 mM HEPES in phenol red free DMEM), and mitochondria stained with 25 nM TMRM for 30 min at 37ºC prior to imaging (TMRM retained in buffer throughout imaging). Cells were imaged immediately using a Leica SP8 confocal microscope and LAS X software platform at 37ºC, using 488 and 562 nm laser lines.

Live Cell Spinning Disk Microscopy

Cells were seeded onto 35 mm glass bottomed dishes (Corning). Immediately prior to imaging, cells were incubated with MitoTracker Green for 30 min at 37ºC, washed three times in HBSS and transferred into imaging media (as above). Imaging was performed using an Olympus IXplore SpinSR system at 37ºC, using 488 and 561 nm laser lines. A z-stack was taken with 10 z-slices, taken at regular intervals (see figure legend).

Live Cell Structured Illumination Microscopy

Transfected cells were grown to confluency on glass coverslips prior to staining with 100 nM MitoTracker Green™ for 30 min at 37ºC in complete growth medium. Coverslips were washed in HBSS and incubated in complete growth medium in Attofluor™ Cell Chambers (Invitrogen) for live imaging using super-resolution 3D structured illumination microscopy (SR-3D SIM) on an OMX v4 microscope (GE Healthcare) at 37ºC, using 488 and 568 nm laser lines and a 60x objective.

Light Microscopy Image Analysis

All image analysis was performed using the FiJi image processing package [63, 64]. Macros were written by Dr Stephen Cross (Wolfson Bioimaging Facility, University of Bristol), within the FiJi plugin Modular Image Analysis (MIA) package version 0.21.0, which is publicly accessible on GitHub with a linked version

specific DOI from Zenodo [65]. Where data was analysed manually, data was randomised/blinded prior to manual analysis.

Mitochondrial pre-processing, as well as branch and network analysis was carried out as described previously [66, 67], using a FiJi plugin adapted from the mitochondrial network analysis (MiNA) toolset [68]. Briefly, for pre-processing, cells of interest were outlined and outside cleared, prior to z-stack max intensity projection, contrast enhancement and background subtraction. Median, unsharp, and tubeness filters were applied. For branch/network analysis, images were binarised and skeletonised, and the skeleton analysed to obtain information on the branches and pixels, allowing analysis of mitochondrial branching as a readout of mitochondrial network complexity and fragmentation.

Analysis of mitochondrial width was carried out by manual measurement. Data was blinded and the same region of mitochondria was measured in each cell (100 x 100 pixels at 2 'o' clock relative to the nucleus) to maintain unbiased results. Five measurements were taken across each mitochondrion (parallel to cristae) and averaged to obtain an average width for the given mitochondrion. An equal number of mitochondria were analysed for each condition.

Circularity analysis was carried out using a macro that classifies mitochondria based on their shape, providing a circularity index, where a value of 1 represents a perfect circle.

Aggregation analysis was carried out using a macro, on images acquired by SIM. Mitochondria (channel 1) are detected in 2D within a region of interest (ROI, *i.e.,* a transfected cell) and the pixel intensity of the trapping substrate (channel 2) is measured as a 4-pixel wide strip at the edge of the mitochondrion. The background channel 2 intensity (intensity at 10-14 pixels from the edge of the mitochondrion) is subtracted from the raw intensity surrounding the mitochondrion, to account for differing expression levels between cells. This provides values for the intensity directly surrounding mitochondria, and after thresholding, these values highlight the proportion of mitochondria within a cell or population of cells that have trapped protein on their outside.

<u>NanoLuc Assay</u>

NanoLuc assays were carried out exactly as described previously [21]. Briefly, cells on standard white flat-bottom 96-well plates were washed with HBSS and incubated in HBSS imaging buffer (HBSS supplemented with 5 mM D-(+)-glucose,10 mM HEPES (Santa Cruz Biotechnology, Germany), 1 mM $MgCl_2$, 1 mM $CaCl_2$; pH 7.4). A fluorescence read was taken at 605/670 nm using monochromators with gain set to allow maximum sensitivity without saturation, using a BioTek Synergy Neo2 plate reader

(Agilent, UK). Cells were transferred to permeabilised cell assay master mix (225 mM mannitol, 10 mM HEPES, 2.5 mM $MgCl_2$, 40 mM KCl, 2.5 mM KH_2PO_4, 0.5 mM EGTA; pH 7.4) supplemented with 5 mM succinate, 1 µM rotenone, 0.1 mg/mL creatine kinase, 5 mM creatine phosphate, 1 mM ATP, 0.1% (v/v) Prionex, 3 nM rPFO (purified in house), 20 µM GST-Dark (purified in house), 1:800 furimazine (Nano-Glo® Luciferase Assay System; Promega). A baseline read of 30 seconds of background luminescent signal was taken prior to injection of purified substrate protein (*Su9-EGFP-pep86*) to 1 µM final concentration, followed by a further bioluminescence read corresponding to import, lasting 30 min. Bioluminescence was read using a BioTek Synergy Neo2 plate reader or a CLARIOstar Plus plate reader (BMG LabTech, UK) without emission filters with gain set to allow maximum sensitivity without saturation, and with acquisition time of 0.1 sec per well. Row mode was used, and reads were taken every 6 sec or less, with wells in triplicate.

Statistical Analysis

Statistical significance between groups was determined using unpaired Student's t-Test or one and two-way ANOVA with interaction if more than two groups were analysed. ANOVA was nested if multiple objects were analysed per biological replicate. Following ANOVA, p values were adjusted for multiple comparisons through Tukey's *post-hoc* test and differences were considered significant at 5% level. Statistical analyses were performed using Graph Pad Prism version 9 (GraphPad Software, Inc., San Diego, CA, USA).

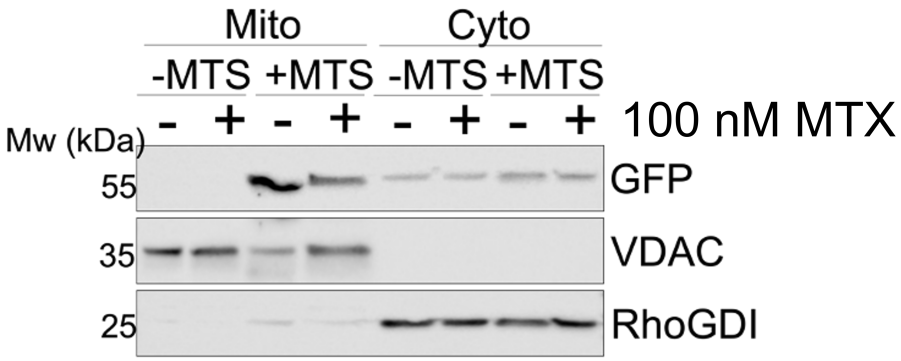

Fig. S1.

Representative Western blot showing expression (48 h) of *EGFP-DHFR* (-MTS) or *Su9-EGFP-DHFR* (+MTS) in the cytosolic and crude mitochondrial fractions of HeLaGAL cells in the presence or absence of 100 nM MTX (48 h). The abundance of *EGFP-DHFR* or *Su9-EGFP-DHFR* in each fraction was visualised by probing with an anti-GFP antibody (Sigma; G1544). VDAC (Invitrogen; PA1-954A) was used as a mitochondrial loading control and RhoGDI (Abcam; ab133248) was used as a cytosolic loading control. N=4 biological replicates.

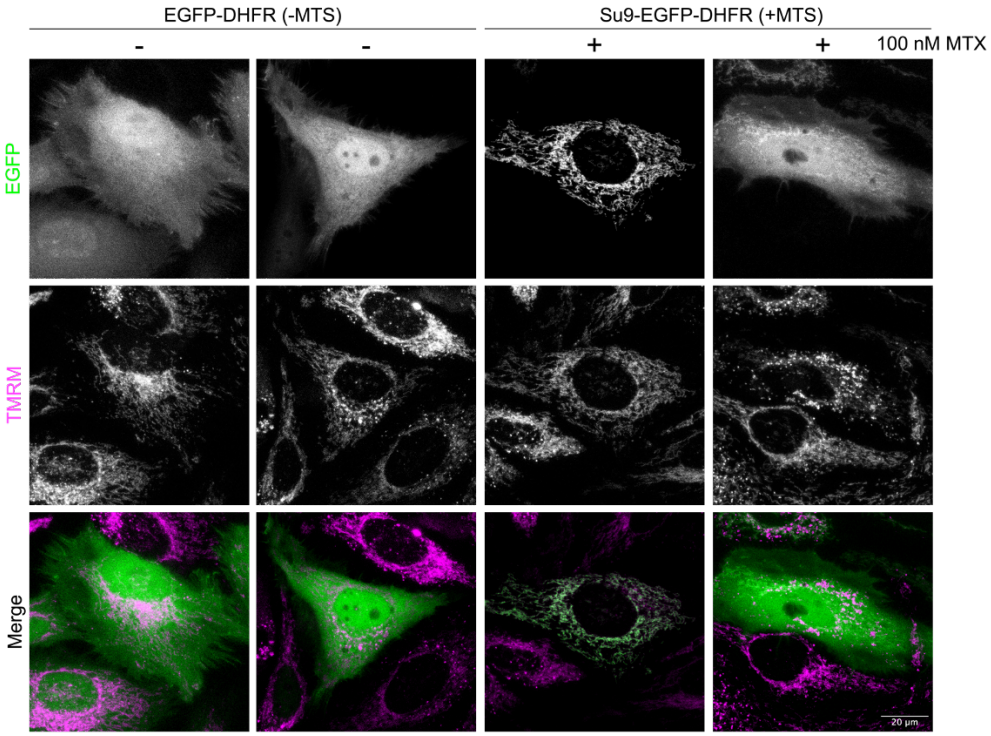

Fig. S2.

Representative confocal images of HeLaGAL cells treated with 100 nM MTX (or with vehicle; DMSO only) overnight prior to expression of *EGFP-DHFR* (-MTS; green) or *Su9-EGFP-DHFR* (+MTS; green) for 48 hours. Mitochondria were stained with 25 nM TMRM (magenta). Overlay shows cellular *EGFP-DHFR* or *Su9-EGFP-DHFR* localisation. N=3 biological replicates.

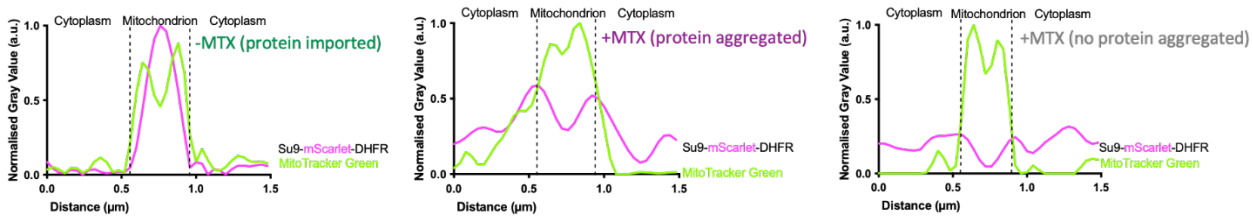

Fig. S3.

Representative plots of average pixel intensity across a mitochondrion in cells subjected to the trapping insult with (middle panel) or without (right) associated trapped precursor, or in cells not treated with MTX (with imported precursor; left panel).

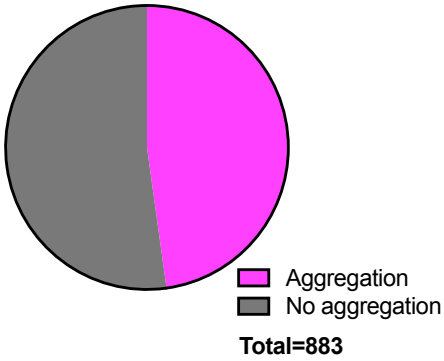

Fig. S4.

Quantification of the proportion of mitochondria per cell with (magenta) or without (grey) trapped precursor surrounding them. Analysis was done using a FiJi plugin as described in methods. N=3 biological replicates. Analysis included a total of 883 mitochondria.

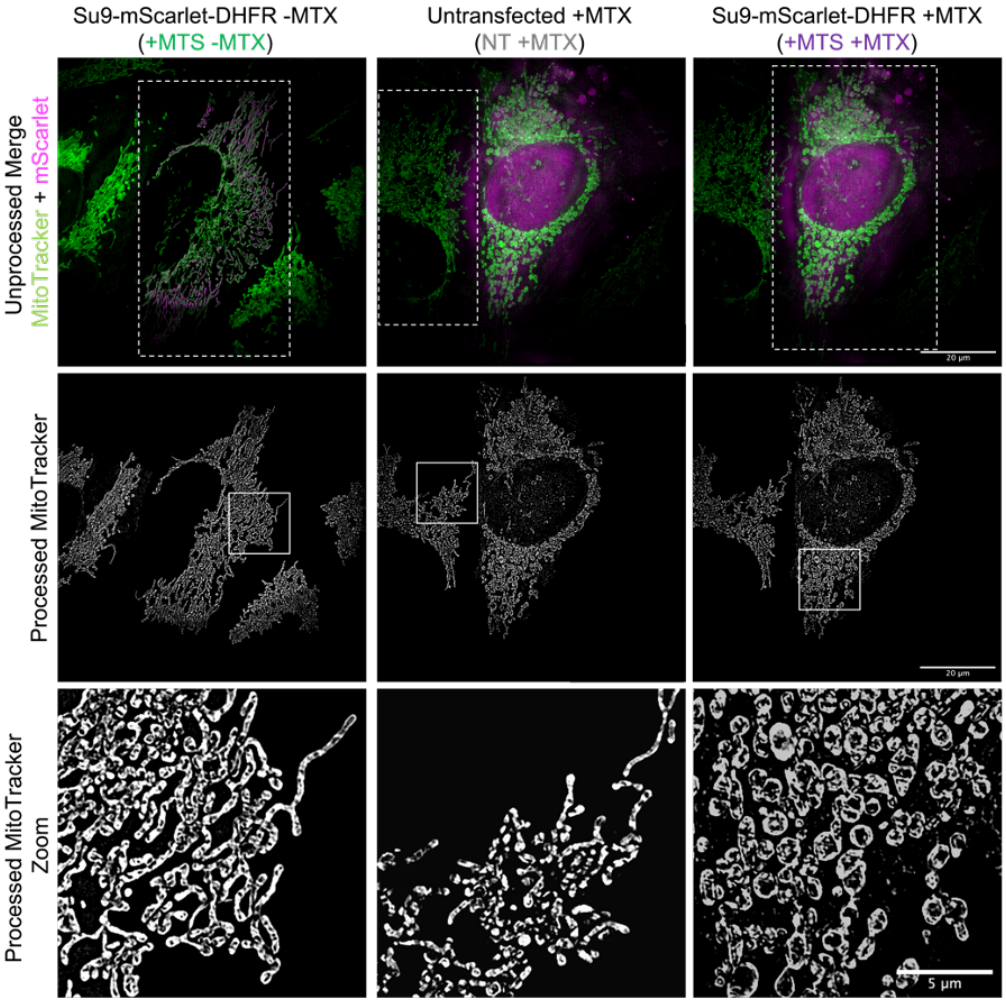

Fig. S5.

Representative SR 3D-SIM images showing mitochondria in HeLaGAL cells subjected to trapping (+MTS +MTX) or not (+MTS -MTX). Untransfected cells in the same well as cells subjected to trapping were used as an internal control for MTX treatment (NT +MTX). The top row shows a merge of MitoTracker Green (green) and mScarlet (magenta) prior to pre-processing. The middle row shows mitochondria (MitoTracker Green channel only) after pre-processing (described in methods). The bottom panel shows a zoom of an area of mitochondria (highlighted in the middle panel) to give a clearer view of mitochondrial morphology. N=3 biological repeats.

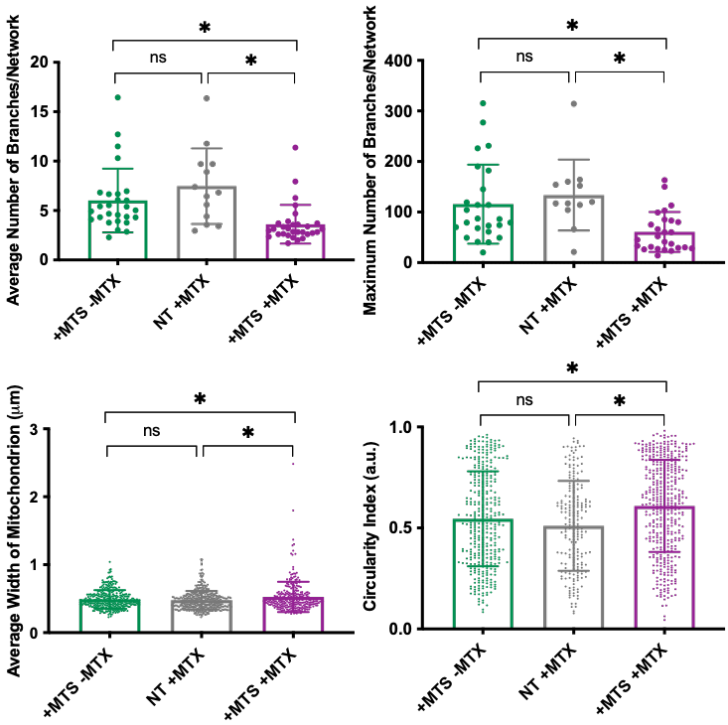

Fig. S6.

Quantification of mitochondrial morphology in terms of branching, width, and circularity. This was carried out for cells expressing *Su9-mScarlet-DHFR* in the absence of MTX (imported precursor; +MTS -MTX; green), internal control cells (untransfected but in the presence of 100 nM MTX; NT +MTX; grey), and transfected cells in the presence of MTX (trapped precursor; +MTS +MTX; purple). For *branching*, each point represents an individual cell from a separate field of view. N=27, 13, 30 cells for different conditions, respectively, taken from 3 independent biological repeats (N=3). For *width*, each point represents an individual mitochondrion, as an average of 5 measurements taken for any one mitochondrion, from a region from a selected field of view (independent cell). N=360, 470, 315 mitochondria, from 20 cells for each condition, respectively, taken from 3 independent biological repeats (N=3). For *circularity*, each point represents an individual mitochondrion. N=359, 199, 434 mitochondria, respectively, taken from 3 independent biological repeats (N=3). Error bars show SD. Nested one-way ANOVA and Tukey's *post-hoc* test were used to determine significance.

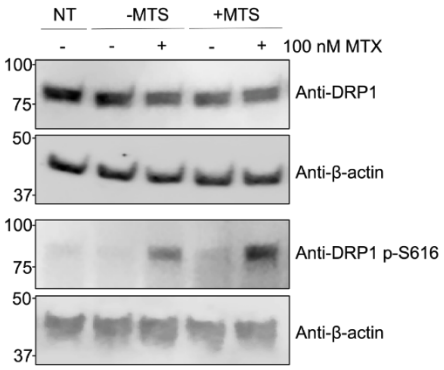

Fig. S7.

Representative Western blots showing abundance of total DRP1 (BD Biosciences; 6111113) or phospho-DRP1 S616 (CST; 4494) in whole cell lysates from HeLa cells expressing *EGFP-DHFR* or *Su9-EGFP-DHFR*, or untransduced (NT) cells in the absence of presence of 100 nM MTX. β-actin (Sigma; A2228) was used as a loading control. N=3 biological replicates.

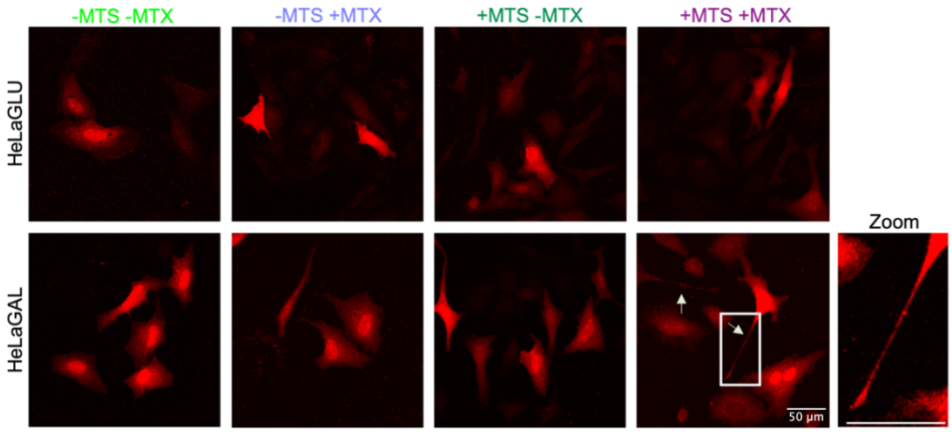

Fig. S8.

Representative confocal images showing morphology of HeLaGLU or HeLaGAL cells subjected to expression of *mCherry* (red) as well as *EGFP-DHFR* (-MTS) or *Su9-EGFP-DHFR* (+MTS) in the absence or presence of 100 nM MTX. Arrows point to protrusions, and box highlights region of interest displayed in zoom. N=4 biological replicates.

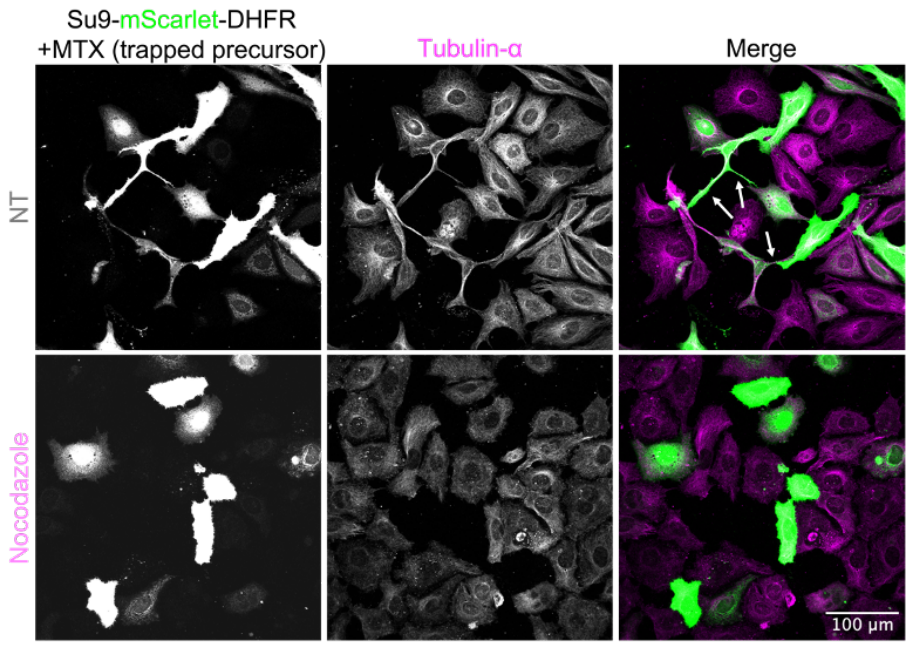

Fig. S9.

Representative confocal images of HeLaGAL cells exposed to precursor trapping in the absence or presence of TNT inhibitor nocodazole. HeLaGAL cells were subjected to trapping (*Su9-mScarlet-DHFR* +100 nM MTX; green) and either untreated (NT; DMSO only) or treated with 100 nM Nocodazole for 48 h (duration of precursor trapping). Cells were fixed and stained for tubulin-α (magenta; BioRad MCA78G) to visualise TNTs. N=3 biological replicates.

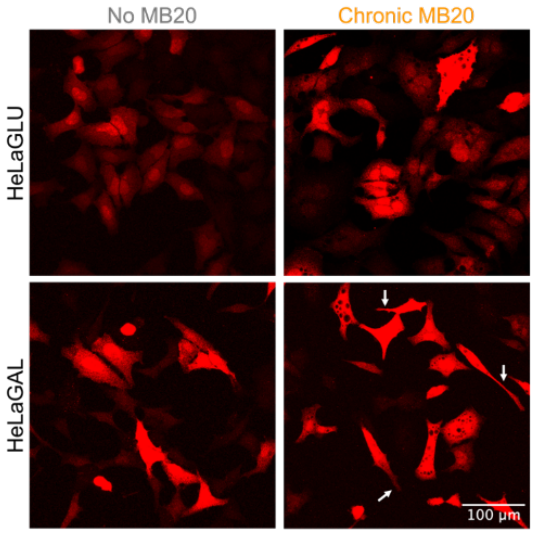

Fig. S10.

Representative images demonstrating morphology (shown by overexpressed *mCherry* cytosolic marker; red) of HeLaGLU or HeLaGAL cells treated with 10 µM MB20 for 48 h, visualised by confocal microscopy. Arrows highlight TNTs. N=6 biological replicates.

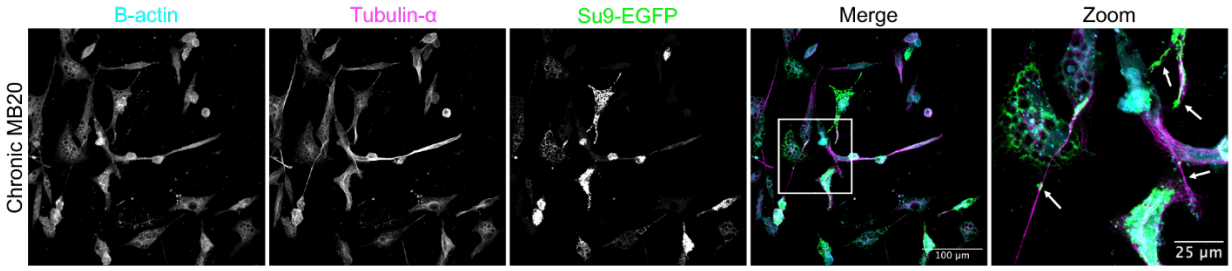

Fig. S11.

Representative images showing composition of MB20-induced protrusions. Cells expressing *Su9-EGFP* (mitochondrial marker; green) were treated for 48 h with 10 µM MB20. Fixed cells were stained for β-actin (cyan; Sigma A2228) and tubulin-α (magenta; BioRad MCA78G). Box shows zoom area and arrows in zoom highlight TNTs. N=3 biological replicates.

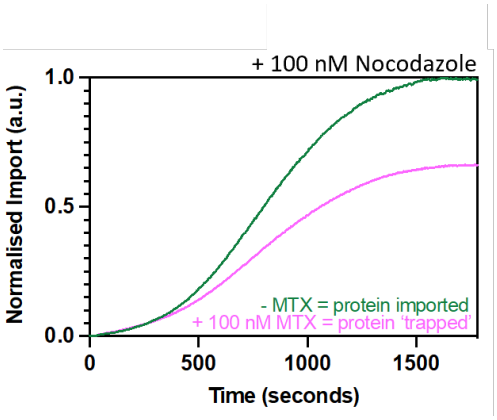

Fig. S12.

NanoLuc import trace showing the impact of TNT inhibitor nocodazole on import of a precursor protein in HeLaGAL cells subjected to precursor trapping. Cells were subjected to trapping (+MTX; pink) or not (-MTX; green) in the presence of 100 nM Nocodazole for 48 h prior to monitoring the import of *Su9-EGFP-pep86* by NanoLuc import assays. N=3 biological replicates, each with n=3 technical replicates.

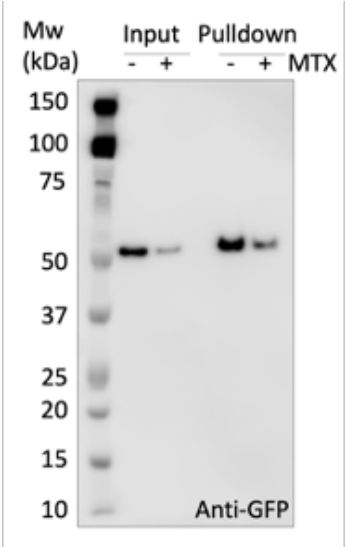

Fig. S13.

Representative Western blot showing GFP-tagged protein in the input and pulldown samples. Samples were prepared as described in schematic in Fig. 4D and probed against a GFP antibody (Sigma; G1544) to validate IP. N=3 biological replicates.

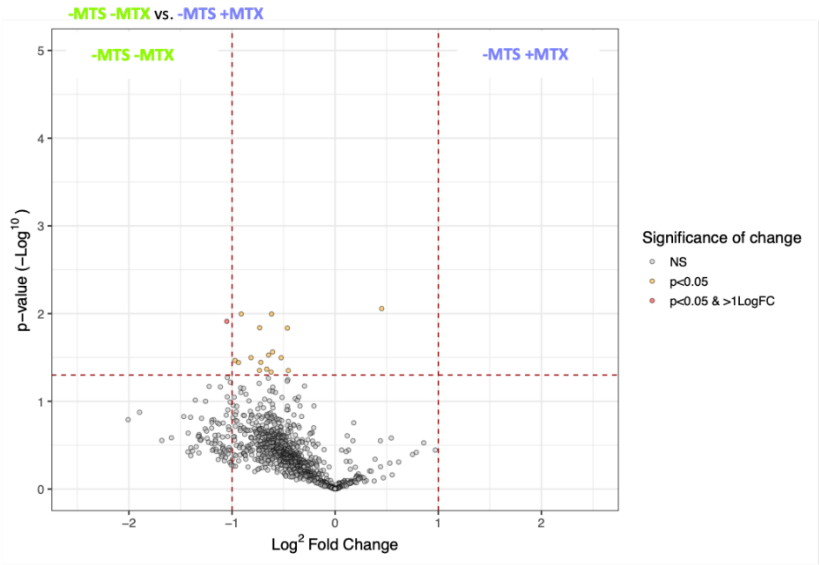

Fig. S14.

Volcano plot highlighting proteins enhanced in pulldown samples from mitochondria of cells overexpressing *EGFP-DHFR* (-MTS) in the presence or absence of 100 nM MTX, to control for background effect of MTX. N=3 biological replicates.

Gene	Protein	Log FC	T-Test
ADAR	Double-stranded RNA-specific adenosine deaminase (DRADA) (EC 3.5.4.37) (136 kDa double-stranded RNA-binding protein) (p136) (Interferon-inducible protein 4) (IFI-4) (K88DSRBP)	0.44	3.84E-05
PPP2R2A	Serine/threonine-protein phosphatase 2A 55 kDa regulatory subunit B alpha isoform (PP2A subunit B isoform B55-alpha) (PP2A subunit B isoform PR55-alpha) (PP2A subunit B isoform R2-alpha) (PP2A subunit B isoform alpha)	0.23	1.35E-04
MTG1	Mitochondrial ribosome-associated GTPase 1 (GTP-binding protein 7) (Mitochondrial GTPase 1)	0.62	4.31E-04
PLOD2	Procollagen-lysine,2-oxoglutarate 5-dioxygenase 2 (EC 1.14.11.4) (Lysyl hydroxylase 2) (LH2)	0.79	5.34E-04
RPRD1A	Regulation of nuclear pre-mRNA domain-containing protein 1A (Cyclin-dependent kinase inhibitor 2B-related protein) (p15INK4B-related protein)	0.66	5.62E-04
MYOF	Myoferlin (Fer-1-like protein 3)	0.53	7.52E-04
SMCHD1	Structural maintenance of chromosomes flexible hinge domain-containing protein 1 (SMC hinge domain-containing protein 1) (EC 3.6.1.-)	0.57	9.86E-04
TARDBP	TAR DNA-binding protein 43 (TDP-43)	0.58	1.04E-03
PDK1	[Pyruvate dehydrogenase (acetyl-transferring)] kinase isozyme 1, mitochondrial (EC 2.7.11.2) (Pyruvate dehydrogenase kinase isoform 1) (PDH kinase 1)	0.74	1.15E-03
FMR1	Synaptic functional regulator FMR1 (Fragile X mental retardation protein 1) (FMRP) (Protein FMR-1)	0.40	1.17E-03
ACOT8	Acyl-coenzyme A thioesterase 8 (Acyl-CoA thioesterase 8) (EC 3.1.2.1) (EC 3.1.2.11) (EC 3.1.2.2) (EC 3.1.2.3) (EC 3.1.2.5) (Choloyl-coenzyme A thioesterase) (EC 3.1.2.27) (HIV-Nef-associated acyl-CoA thioesterase) (Peroxisomal acyl-CoA thioesterase 2) (PTE-2) (Peroxisomal acyl-coenzyme A thioester hydrolase 1) (PTE-1) (Peroxisomal long-chain acyl-CoA thioesterase 1) (Thioesterase II) (hACTE-III) (hACTEIII) (hTE)	0.55	1.24E-03
S100A2	Protein S100-A2 (CAN19) (Protein S-100L) (S100 calcium-binding protein A2)	0.84	1.25E-03
CFL1	Cofilin-1 (18 kDa phosphoprotein) (p18) (Cofilin, non-muscle isoform)	0.56	1.46E-03
	cDNA FLJ55806, highly similar to Golgi phosphoprotein 3	0.76	1.74E-03
TRIM25	E3 ubiquitin/ISG15 ligase TRIM25 (EC 6.3.2.n3) (Estrogen-responsive finger protein) (RING finger protein 147) (RING-type E3 ubiquitin transferase) (EC 2.3.2.27) (RING-type E3 ubiquitin transferase TRIM25) (Tripartite motif-containing protein 25) (Ubiquitin/ISG15-conjugating enzyme TRIM25) (Zinc finger protein 147)	0.36	2.05E-03
GSTM3	Glutathione S-transferase Mu 3 (EC 2.5.1.18) (GST class-mu 3) (GSTM3-3) (hGSTM3-3)	0.61	2.22E-03
RPL11	60S ribosomal protein L11 (CLL-associated antigen KW-12) (Large ribosomal subunit protein uL5)	0.28	2.78E-03
RCN2	Reticulocalbin-2 (Calcium-binding protein ERC-55) (E6-binding protein) (E6BP)	0.26	3.25E-03
RPL30	60S ribosomal protein L30 (Large ribosomal subunit protein eL30)	0.46	3.37E-03

PDP1	[Pyruvate dehydrogenase [acetyl-transferring]]-phosphatase 1, mitochondrial (PDP 1) (EC 3.1.3.43) (Protein phosphatase 2C) (Pyruvate dehydrogenase phosphatase catalytic subunit 1) (PDPC 1)	0.71	3.55E-03
ALDH3A2	Aldehyde dehydrogenase family 3 member A2 (EC 1.2.1.3) (EC 1.2.1.94) (Aldehyde dehydrogenase 10) (Fatty aldehyde dehydrogenase) (Microsomal aldehyde dehydrogenase)	0.50	3.65E-03
VPS26C	Vacuolar protein sorting-associated protein 26C (Down syndrome critical region protein 3) (Down syndrome critical region protein A)	0.39	3.91E-03
PARK7	Parkinson disease protein 7 (Maillard deglycase) (Oncogene DJ1) (Parkinsonism-associated deglycase) (Protein DJ-1) (DJ-1) (Protein/nucleic acid deglycase DJ-1) (EC 3.1.2.-) (EC 3.5.1.-) (EC 3.5.1.124)	0.58	3.93E-03
LYRM7	Complex III assembly factor LYRM7 (LYR motif-containing protein 7)	0.66	3.94E-03
GFM2	Ribosome-releasing factor 2, mitochondrial (RRF2mt) (Elongation factor G 2, mitochondrial) (EF-G2mt) (mEF-G 2) (Elongation factor G2) (hEFG2)	0.39	4.00E-03
FARS2	Phenylalanine--tRNA ligase, mitochondrial (EC 6.1.1.20) (Phenylalanyl-tRNA synthetase) (PheRS)	0.60	4.11E-03
TBC1D24	TBC1 domain family member 24	0.78	4.13E-03
SH3GL1	Endophilin-A2 (EEN fusion partner of MLL) (Endophilin-2) (Extra eleven-nineteen leukemia fusion gene protein) (EEN) (SH3 domain protein 2B) (SH3 domain-containing GRB2-like protein 1)	0.68	4.27E-03
RECQL	ATP-dependent DNA helicase Q1 (EC 3.6.4.12) (DNA helicase, RecQ-like type 1) (RecQ1) (DNA-dependent ATPase Q1) (RecQ protein-like 1)	0.45	4.47E-03
C1QBP	Complement component 1 Q subcomponent-binding protein, mitochondrial (ASF/SF2-associated protein p32) (Glycoprotein gC1qBP) (C1qBP) (Hyaluronan-binding protein 1) (Mitochondrial matrix protein p32) (gC1q-R protein) (p33) (SF2AP32)	0.35	4.72E-03
CLCC1	Chloride channel CLIC-like protein 1 (Mid-1-related chloride channel protein 1)	1.03	4.99E-03
BUB3	Mitotic checkpoint protein BUB3	0.34	5.11E-03
DDX5	Probable ATP-dependent RNA helicase DDX5 (EC 3.6.4.13) (DEAD box protein 5) (RNA helicase p68)	0.40	5.22E-03
LANCL1	Glutathione S-transferase LANCL1 (EC 2.5.1.18) (40 kDa erythrocyte membrane protein) (p40) (LanC-like protein 1)	0.64	5.47E-03
LAMP1	Lysosome-associated membrane glycoprotein 1 (LAMP-1) (Lysosome-associated membrane protein 1) (CD107 antigen-like family member A) (CD antigen CD107a)	0.57	5.52E-03
HNRNPA3	Heterogeneous nuclear ribonucleoprotein A3 (hnRNP A3)	0.84	5.55E-03
EEF1A1	Elongation factor 1-alpha 1 (EF-1-alpha-1) (Elongation factor Tu) (EF-Tu) (Eukaryotic elongation factor 1 A-1) (eEF1A-1) (Leukocyte receptor cluster member 7)	0.17	5.58E-03
SRPRB	Signal recognition particle receptor subunit beta (SR-beta) (Protein APMCF1)	0.50	5.65E-03
DDX3X	ATP-dependent RNA helicase DDX3X (EC 3.6.4.13) (CAP-Rf) (DEAD box protein 3, X-chromosomal) (DEAD box, X isoform) (DBX) (Helicase-like protein 2) (HLP2)	0.31	5.73E-03

DSC3	Desmocollin-3 (Cadherin family member 3) (Desmocollin-4) (HT-CP)	0.58	6.02E-03
AUP1	Lipid droplet regulating VLDL assembly factor AUP1 (Ancient ubiquitous protein 1)	0.56	6.12E-03
PSMB5	Proteasome subunit beta type-5 (EC 3.4.25.1) (Macropain epsilon chain) (Multicatalytic endopeptidase complex epsilon chain) (Proteasome chain 6) (Proteasome epsilon chain) (Proteasome subunit MB1) (Proteasome subunit X)	0.69	6.21E-03
	Dynamin-like 120 kDa protein, mitochondrial (EC 3.6.5.5)	0.69	6.97E-03
GNA14	Guanine nucleotide-binding protein subunit alpha-14 (G alpha-14) (G-protein subunit alpha-14)	0.51	7.33E-03
RPN1	Dolichyl-diphosphooligosaccharide--protein glycosyltransferase subunit 1 (Dolichyl-diphosphooligosaccharide--protein glycosyltransferase 67 kDa subunit) (Ribophorin I) (RPN-I) (Ribophorin-1)	0.61	7.36E-03
PMPCA	Mitochondrial-processing peptidase subunit alpha (Alpha-MPP) (Inactive zinc metalloprotease alpha) (P-55)	0.47	7.76E-03
	cDNA FLJ90170 fis, clone MAMMA1000370, highly similar to Ig alpha-1 chain C region	0.79	7.79E-03
CALU	Calumenin (Crocalbin) (IEF SSP 9302)	0.55	8.11E-03
LANCL2	LanC-like protein 2 (Testis-specific adriamycin sensitivity protein)	0.69	8.12E-03
RAB5C	Ras-related protein Rab-5C (EC 3.6.5.2) (L1880) (RAB5L)	0.96	8.49E-03
PPOX	Protoporphyrinogen oxidase (PPO) (EC 1.3.3.4)	0.46	8.71E-03
RTCB	RNA-splicing ligase RtcB homolog (EC 6.5.1.8) (3'-phosphate/5'-hydroxy nucleic acid ligase)	0.30	8.94E-03
LYPLA1	Acyl-protein thioesterase 1 (APT-1) (hAPT1) (EC 3.1.2.-) (Lysophospholipase 1) (Lysophospholipase I) (LPL-I) (LysoPLA I) (Palmitoyl-protein hydrolase) (EC 3.1.2.22)	0.58	8.99E-03
CSNK1D	Casein kinase I isoform delta (CKI-delta) (CKId) (EC 2.7.11.1) (Tau-protein kinase CSNK1D) (EC 2.7.11.26)	0.64	9.24E-03
B4GALT1	Beta-1,4-galactosyltransferase 1 (Beta-1,4-GalTase 1) (Beta4Gal-T1) (b4Gal-T1) (EC 2.4.1.-) (Beta-N-acetylglucosaminyl-glycolipid beta-1,4-galactosyltransferase) (Beta-N-acetylglucosaminylglycopeptide beta-1,4-galactosyltransferase) (EC 2.4.1.38) (Lactose synthase A protein) (EC 2.4.1.22) (N-acetyllactosamine synthase) (EC 2.4.1.90) (Nal synthase) (Neolactotriaosylceramide beta-1,4-galactosyltransferase) (EC 2.4.1.275) (UDP-Gal:beta-GlcNAc beta-1,4-galactosyltransferase 1) (UDP-galactose:beta-N-acetylglucosamine beta-1,4-galactosyltransferase 1) [Cleaved into: Processed beta-1,4-galactosyltransferase 1]	0.88	9.26E-03
HNRNPK	Heterogeneous nuclear ribonucleoprotein K (hnRNP K) (Transformation up-regulated nuclear protein) (TUNP)	0.65	9.51E-03
RAB34	Ras-related protein Rab-34 (Ras-related protein Rab-39) (Ras-related protein Rah)	0.41	9.58E-03
LYPLAL1	Lysophospholipase-like protein 1 (EC 3.1.2.22)	0.69	9.60E-03
FN1	Fibronectin (FN) (Cold-insoluble globulin) (CIG) [Cleaved into: Anastellin; Ugl-Y1; Ugl-Y2; Ugl-Y3]	1.12	9.72E-03
NSF	Vesicle-fusing ATPase (EC 3.6.4.6) (N-ethylmaleimide-sensitive fusion protein) (NEM-sensitive fusion protein) (Vesicular-fusion protein NSF)	0.72	9.97E-03

DNAJC7	DnaJ homolog subfamily C member 7 (Tetratricopeptide repeat protein 2) (TPR repeat protein 2)	0.65	9.98E-03
RNPC3	RNA-binding region-containing protein 3 (RNA-binding motif protein 40) (RNA-binding protein 40) (U11/U12 small nuclear ribonucleoprotein 65 kDa protein) (U11/U12 snRNP 65 kDa protein) (U11/U12-65K)	0.56	1.00E-02
ACAA1	3-ketoacyl-CoA thiolase, peroxisomal (EC 2.3.1.16) (Acetyl-CoA C-myristoyltransferase) (EC 2.3.1.155) (Acetyl-CoA acyltransferase) (EC 2.3.1.9) (Beta-ketothiolase) (Peroxisomal 3-oxoacyl-CoA thiolase)	0.78	1.05E-02
AK2	Adenylate kinase 2, mitochondrial (AK 2) (EC 2.7.4.3) (ATP-AMP transphosphorylase 2) (ATP: AMP phosphotransferase) (Adenylate monophosphate kinase) [Cleaved into: Adenylate kinase 2, mitochondrial, N-terminally processed]	0.73	1.08E-02
ILVBL	2-hydroxyacyl-CoA lyase 2 (EC 4.1.2.-) (Acetolactate synthase-like protein) (IlvB-like protein)	0.69	1.08E-02
IMPA2	Inositol monophosphatase 2 (IMP 2) (IMPase 2) (EC 3.1.3.25) (Inositol-1(or 4)-monophosphatase 2) (Myo-inositol monophosphatase A2)	0.41	1.09E-02
GALNT2	Polypeptide N-acetylgalactosaminyltransferase 2 (EC 2.4.1.41) (Polypeptide GalNAc transferase 2) (GalNAc-T2) (pp-GaNTase 2) (Protein-UDP acetylgalactosaminyltransferase 2) (UDP-GalNAc: polypeptide N-acetylgalactosaminyltransferase 2) [Cleaved into: Polypeptide N-acetylgalactosaminyltransferase 2 soluble form]	0.74	1.10E-02
MAGT1	Magnesium transporter protein 1 (MagT1) (Dolichyl-diphosphooligosaccharide--protein glycosyltransferase subunit MAGT1) (Oligosaccharyl transferase subunit MAGT1) (Implantation-associated protein) (IAP)	0.70	1.11E-02
TK2	Thymidine kinase 2, mitochondrial (EC 2.7.1.21) (2'-deoxyuridine kinase TK2) (EC 2.7.1.74) (Deoxycytidine kinase TK2) (EC 2.7.1.-) (Mt-TK)	0.75	1.16E-02
MRPS6	28S ribosomal protein S6, mitochondrial (MRP-S6) (S6mt) (Mitochondrial small ribosomal subunit protein bS6m)	0.78	1.16E-02
ACTA2	Actin, aortic smooth muscle (Alpha-actin-2) (Cell growth-inhibiting gene 46 protein) [Cleaved into: Actin, aortic smooth muscle, intermediate form]	-0.08	1.19E-02
PRORP	Mitochondrial ribonuclease P catalytic subunit (EC 3.1.26.5) (Mitochondrial ribonuclease P protein 3) (Mitochondrial RNase P protein 3) (Protein only RNase P catalytic subunit)	0.65	1.22E-02
KIF2C	Kinesin-like protein KIF2C (Kinesin-like protein 6) (Mitotic centromere-associated kinesin) (MCAK)	0.47	1.23E-02
SPART	Spartin (Spastic paraplegia 20 protein) (Trans-activated by hepatitis C virus core protein 1)	0.35	1.23E-02
PHLDA3	Pleckstrin homology-like domain family A member 3 (TDAG51/Ipl homolog 1)	0.63	1.24E-02
ATP2B4	Plasma membrane calcium-transporting ATPase 4 (PMCA4) (EC 7.2.2.10) (Matrix-remodeling-associated protein 1) (Plasma membrane calcium ATPase isoform 4) (Plasma membrane calcium pump isoform 4)	0.60	1.25E-02
STARD7	StAR-related lipid transfer protein 7, mitochondrial (Gestational trophoblastic tumor protein 1) (START domain-containing protein 7) (StARD7)	0.86	1.27E-02

	cDNA FLJ58476, highly similar to Poly(rC)-binding protein 2	0.29	1.30E-02
HACL1	2-hydroxyacyl-CoA lyase 1 (EC 4.1.2.63) (2-hydroxyphytanoyl-CoA lyase) (2-HPCL) (Phytanoyl-CoA 2-hydroxylase 2)	0.84	1.30E-02
SSR4	Translocon-associated protein subunit delta (TRAP-delta) (Signal sequence receptor subunit delta) (SSR-delta)	0.84	1.34E-02
INPP5K	Inositol polyphosphate 5-phosphatase K (EC 3.1.3.56) (Phosphatidylinositol-3,4,5-trisphosphate 5-phosphatase) (EC 3.1.3.86) (Phosphatidylinositol-4,5-bisphosphate 5-phosphatase) (EC 3.1.3.36) (Skeletal muscle and kidney-enriched inositol phosphatase)	0.24	1.34E-02
PTBP1	Polypyrimidine tract-binding protein 1 (PTB) (57 kDa RNA-binding protein PPTB-1) (Heterogeneous nuclear ribonucleoprotein I) (hnRNP I)	0.48	1.43E-02
TRIO	Triple functional domain protein (EC 2.7.11.1) (PTPRF-interacting protein)	0.65	1.44E-02
ARG1	Arginase-1 (EC 3.5.3.1) (Liver-type arginase) (Type I arginase)	0.69	1.45E-02
HNRNPL	Heterogeneous nuclear ribonucleoprotein L (hnRNP L)	0.67	1.45E-02
GNPAT	Dihydroxyacetone phosphate acyltransferase (DAP-AT) (DHAP-AT) (EC 2.3.1.42) (Acyl-CoA: dihydroxyacetonephosphateacyl transferase) (Glycerone-phosphate O-acyltransferase)	0.47	1.46E-02
DDX47	Probable ATP-dependent RNA helicase DDX47 (EC 3.6.4.13) (DEAD box protein 47)	0.53	1.48E-02
ACTN4	Alpha-actinin-4 (non-muscle alpha-actinin 4)	0.35	1.49E-02
MYL12B	Myosin regulatory light chain 12B (MLC-2A) (MLC-2) (Myosin regulatory light chain 2-B, smooth muscle isoform) (Myosin regulatory light chain 20 kDa) (MLC20) (Myosin regulatory light chain MRLC2) (SHUJUN-1)	0.23	1.49E-02
FECH	Ferrochelatase, mitochondrial (EC 4.99.1.1) (Heme synthase) (Protoheme ferro-lyase)	0.67	1.51E-02
TPD52L2	Tumor protein D54 (hD54) (Tumor protein D52-like 2)	0.61	1.55E-02
HTATIP2	Oxidoreductase HTATIP2 (EC 1.1.1.-) (30 kDa HIV-1 TAT-interacting protein) (HIV-1 TAT-interactive protein 2)	0.57	1.56E-02
DHRS7B	Dehydrogenase/reductase SDR family member 7B (EC 1.1.-.-) (Short-chain dehydrogenase/reductase family 32C member 1) (Protein SDR32C1)	0.43	1.57E-02
AIFM2	Ferroptosis suppressor protein 1 (FSP1) (EC 1.6.5.-) (Apoptosis-inducing factor homologous mitochondrion-associated inducer of death) (AMID) (p53-responsive gene 3 protein)	1.12	1.61E-02
PCBP1	Poly(rC)-binding protein 1 (Alpha-CP1) (Heterogeneous nuclear ribonucleoprotein E1) (hnRNP E1) (Nucleic acid-binding protein SUB2.3)	0.37	1.62E-02
TFB2M	Dimethyladenosine transferase 2, mitochondrial (EC 2.1.1.-) (Hepatitis C virus NS5A-transactivated protein 5) (HCV NS5A-transactivated protein 5) (Mitochondrial 12S rRNA dimethylase 2) (Mitochondrial transcription factor B2) (h-mtTFB) (h-mtTFB2) (hTFB2M) (mtTFB2) (S-adenosylmethionine-6-N', N'-adenosyl(rRNA) dimethyltransferase 2)	0.62	1.63E-02

KDELR1	ER lumen protein-retaining receptor 1 (KDEL endoplasmic reticulum protein retention receptor 1) (KDEL receptor 1) (Putative MAPK-activating protein PM23)	0.54	1.65E-02
NUDT16L1	Tudor-interacting repair regulator protein (NUDT16-like protein 1) (Protein syndesmos)	0.61	1.65E-02
DDOST	Dolichyl-diphosphooligosaccharide--protein glycosyltransferase 48 kDa subunit (DDOST 48 kDa subunit) (Oligosaccharyl transferase 48 kDa subunit)	0.51	1.74E-02
ACOT13	Acyl-coenzyme A thioesterase 13 (Acyl-CoA thioesterase 13) (EC 3.1.2.-) (Hotdog-fold thioesterase superfamily member 2) (Palmitoyl-CoA hydrolase) (EC 3.1.2.2) (Thioesterase superfamily member 2) (THEM2) [Cleaved into: Acyl-coenzyme A thioesterase 13, N-terminally processed]	0.66	1.74E-02
YIPF5	Protein YIPF5 (Five-pass transmembrane protein localizing in the Golgi apparatus and the endoplasmic reticulum 5) (Smooth muscle cell-associated protein 5) (SMAP-5) (YIP1 family member 5) (YPT-interacting protein 1 A)	0.47	1.75E-02
COMT	Catechol O-methyltransferase (EC 2.1.1.6)	0.59	1.78E-02
ACO2	Aconitate hydratase, mitochondrial (Aconitase) (EC 4.2.1.3) (Citrate hydro-lyase)	0.60	1.78E-02
MCM5	DNA replication licensing factor MCM5 (EC 3.6.4.12) (CDC46 homolog) (P1-CDC46)	0.86	1.84E-02
RAB18	Ras-related protein Rab-18	0.75	1.86E-02
CPOX	Oxygen-dependent coproporphyrinogen-III oxidase, mitochondrial (COX) (Coprogen oxidase) (Coproporphyrinogenase) (EC 1.3.3.3)	0.85	1.91E-02
DECR2	Peroxisomal 2,4-dienoyl-CoA reductase [(3E)-enoyl-CoA-producing] (pDCR) (EC 1.3.1.124) (2,4-dienoyl-CoA reductase 2) (Short chain dehydrogenase/reductase family 17C member 1)	0.65	1.92E-02
RRM1	Ribonucleoside-diphosphate reductase large subunit (EC 1.17.4.1) (Ribonucleoside-diphosphate reductase subunit M1) (Ribonucleotide reductase large subunit)	0.70	1.94E-02
AZGP1	Zinc-alpha-2-glycoprotein (Zn-alpha-2-GP) (Zn-alpha-2-glycoprotein)	0.82	1.96E-02
PTRH1	Probable peptidyl-tRNA hydrolase (PTH) (EC 3.1.1.29)	0.62	1.98E-02
CAPZA1	F-actin-capping protein subunit alpha-1 (CapZ alpha-1)	0.24	1.98E-02
LMF2	Lipase maturation factor 2 (Transmembrane protein 112B) (Transmembrane protein 153)	0.84	1.99E-02
SPTBN1	Spectrin beta chain, non-erythrocytic 1 (Beta-II spectrin) (Fodrin beta chain) (Spectrin, non-erythroid beta chain 1)	0.76	2.07E-02
GNB2	Guanine nucleotide-binding protein G(I)/G(S)/G(T) subunit beta-2 (G protein subunit beta-2) (Transducin beta chain 2)	0.49	2.13E-02
KHDRBS1	KH domain-containing, RNA-binding, signal transduction-associated protein 1 (GAP-associated tyrosine phosphoprotein p62) (Src-associated in mitosis 68 kDa protein) (Sam68) (p21 Ras GTPase-activating protein-associated p62) (p68)	0.57	2.16E-02
RARS2	Probable arginine--tRNA ligase, mitochondrial (EC 6.1.1.19) (Arginyl-tRNA synthetase) (ArgRS)	0.51	2.17E-02
HNRNPUL2	Heterogeneous nuclear ribonucleoprotein U-like protein 2 (Scaffold-attachment factor A2) (SAF-A2)	0.62	2.18E-02
DGUOK	Deoxyguanosine kinase, mitochondrial (EC 2.7.1.113) (Deoxyadenosine kinase, mitochondrial) (EC 2.7.1.76)	0.56	2.19E-02

PRKDC	DNA-dependent protein kinase catalytic subunit (DNA-PK catalytic subunit) (DNA-PKcs) (EC 2.7.11.1) (DNPK1) (p460)	0.53	2.20E-02
VAPA	Vesicle-associated membrane protein-associated protein A (VAMP-A) (VAMP-associated protein A) (VAP-A) (33 kDa VAMP-associated protein) (VAP-33)	0.34	2.23E-02
FUBP3	Far upstream element-binding protein 3 (FUSE-binding protein 3)	0.46	2.28E-02
MCM3	DNA replication licensing factor MCM3 (EC 3.6.4.12) (DNA polymerase alpha holoenzyme-associated protein P1) (P1-MCM3) (RLF subunit beta) (p102)	1.07	2.28E-02
RBM14	RNA-binding protein 14 (Paraspeckle protein 2) (PSP2) (RNA-binding motif protein 14) (RRM-containing coactivator activator/modulator) (Synaptotagmin-interacting protein) (SYT-interacting protein)	1.23	2.29E-02
SLC27A4	Long-chain fatty acid transport protein 4 (FATP-4) (Fatty acid transport protein 4) (Arachidonate--CoA ligase) (EC 6.2.1.15) (Long-chain-fatty-acid--CoA ligase) (Solute carrier family 27 member 4) (Very long-chain acyl-CoA synthetase 4) (ACSVL4) (EC 6.2.1.-)	0.52	2.30E-02
EIF5B	Eukaryotic translation initiation factor 5B (eIF-5B) (EC 3.6.5.3) (Translation initiation factor IF-2)	0.77	2.35E-02
PDHA1	Pyruvate dehydrogenase E1 component subunit alpha, somatic form, mitochondrial (EC 1.2.4.1) (PDHE1-A type I)	0.64	2.36E-02
HSPA8	Heat shock cognate 71 kDa protein (Fragment)	0.51	2.36E-02
RCC1	Regulator of chromosome condensation (Cell cycle regulatory protein) (Chromosome condensation protein 1)	0.65	2.37E-02
ECI2	Enoyl-CoA delta isomerase 2 (EC 5.3.3.8) (DRS-1) (Delta(3), delta(2)-enoyl-CoA isomerase) (D3, D2-enoyl-CoA isomerase) (Diazepam-binding inhibitor-related protein 1) (DBI-related protein 1) (Dodecenoyl-CoA isomerase) (Hepatocellular carcinoma-associated antigen 88) (Peroxisomal 3,2-trans-enoyl-CoA isomerase) (pECI) (Renal carcinoma antigen NY-REN-1)	0.57	2.39E-02
	Monocarboxylate transporter 1 (Solute carrier family 16 member 1)	0.47	2.42E-02
MMAB	Corrinoid adenosyltransferase (EC 2.5.1.17) (Cob(II)alamin adenosyltransferase) (Cob(II)yrinic acid a, c-diamide adenosyltransferase) (Cobinamide/cobalamin adenosyltransferase) (Methylmalonic aciduria type B protein)	0.75	2.43E-02
NDUFA4	Cytochrome c oxidase subunit NDUFA4 (Complex I-MLRQ) (CI-MLRQ) (NADH-ubiquinone oxidoreductase MLRQ subunit)	0.82	2.44E-02
PRDX3	Thioredoxin-dependent peroxide reductase, mitochondrial (EC 1.11.1.24) (Antioxidant protein 1) (AOP-1) (HBC189) (Peroxiredoxin III) (Prx-III) (Peroxiredoxin-3) (Protein MER5 homolog) (Thioredoxin-dependent peroxiredoxin 3)	0.77	2.46E-02
RTN3	Reticulon-3 (Homolog of ASY protein) (HAP) (Neuroendocrine-specific protein-like 2) (NSP-like protein 2) (Neuroendocrine-specific protein-like II) (NSP-like protein II) (NSPLII)	0.67	2.49E-02
PMPCB	Mitochondrial-processing peptidase subunit beta (EC 3.4.24.64) (Beta-MPP) (P-52)	0.66	2.51E-02

ATP6V1E1	V-type proton ATPase subunit E 1 (V-ATPase subunit E 1) (V-ATPase 31 kDa subunit) (p31) (Vacuolar proton pump subunit E 1)	0.52	2.51E-02
GSDMA	Gasdermin-A (Gasdermin-1) [Cleaved into: Gasdermin-A, N-terminal (GSDMA-NT); Gasdermin-A, C-terminal (GSDMA-CT)]	0.56	2.54E-02
VMP1	Vacuole membrane protein 1 (Transmembrane protein 49)	0.56	2.54E-02
MTPAP	Poly(A) RNA polymerase, mitochondrial (PAP) (EC 2.7.7.19) (PAP-associated domain-containing protein 1) (Polynucleotide adenylyltransferase) (Terminal uridylyltransferase 1) (TUTase 1) (mtPAP)	0.55	2.55E-02
PCMT1	Protein-L-isoaspartate(D-aspartate) O-methyltransferase (PIMT) (EC 2.1.1.77) (L-isoaspartyl protein carboxyl methyltransferase) (Protein L-isoaspartyl/D-aspartyl methyltransferase) (Protein-beta-aspartate methyltransferase)	0.50	2.56E-02
MAP4	Microtubule-associated protein 4 (MAP-4)	0.42	2.57E-02
CDC42EP1	Cdc42 effector protein 1 (Binder of Rho GTPases 5) (Serum protein MSE55)	0.50	2.62E-02
DPM1	Dolichol-phosphate mannosyltransferase subunit 1 (EC 2.4.1.83) (Dolichol-phosphate mannose synthase subunit 1) (DPM synthase subunit 1) (Dolichyl-phosphate beta-D-mannosyltransferase subunit 1) (Mannose-P-dolichol synthase subunit 1) (MPD synthase subunit 1)	0.60	2.62E-02
CAMK2D	Calcium/calmodulin-dependent protein kinase type II subunit delta (CaM kinase II subunit delta) (CaMK-II subunit delta) (EC 2.7.11.17)	0.68	2.64E-02
PTPRE	Receptor-type tyrosine-protein phosphatase epsilon (Protein-tyrosine phosphatase epsilon) (R-PTP-epsilon) (EC 3.1.3.48)	0.95	2.65E-02
	IG c828_heavy_IGHV3-21_IGHD7-27_IGHJ3 (Fragment)	0.83	2.65E-02
CDK2	Cyclin-dependent kinase 2 (EC 2.7.11.22) (Cell division protein kinase 2) (p33 protein kinase)	0.77	2.65E-02
	AEG2C7 (Fragment)	0.80	2.66E-02
APMAP	Adipocyte plasma membrane-associated protein (Protein BSCv)	0.59	2.68E-02
AGPS	Alkyldihydroxyacetonephosphate synthase, peroxisomal (Alkyl-DHAP synthase) (EC 2.5.1.26) (Aging-associated gene 5 protein) (Alkylglycerone-phosphate synthase)	0.46	2.69E-02
RAN	GTP-binding nuclear protein Ran (Androgen receptor-associated protein 24) (GTPase Ran) (Ras-like protein TC4) (Ras-related nuclear protein)	0.41	2.70E-02
ATP5MK	ATP synthase membrane subunit K, mitochondrial (ATP synthase membrane subunit DAPIT, mitochondrial) (Diabetes-associated protein in insulin-sensitive tissues) (HCV F-transactivated protein 2) (Up-regulated during skeletal muscle growth protein 5)	0.87	2.71E-02
NCKAP1	Nck-associated protein 1 (NAP 1) (Membrane-associated protein HEM-2) (p125Nap1)	0.28	2.71E-02
DNAJA1	DnaJ homolog subfamily A member 1 (DnaJ protein homolog 2) (HSDJ) (Heat shock 40 kDa protein 4) (Heat shock protein J2) (HSJ-2) (Human DnaJ protein 2) (hDj-2)	0.63	2.72E-02
HARS2	Histidine--tRNA ligase, mitochondrial (EC 6.1.1.21) (Histidine--tRNA ligase-like) (Histidyl-tRNA synthetase) (HisRS)	0.53	2.74E-02

TXN	Thioredoxin (Trx) (ATL-derived factor) (ADF) (Surface-associated sulphydryl protein) (SASP) (allergen Hom s Trx)	0.56	2.78E-02
HM13	Minor histocompatibility antigen H13 (EC 3.4.23.-) (Intramembrane protease 1) (IMP-1) (IMPAS-1) (hIMP1) (Presenilin-like protein 3) (Signal peptide peptidase)	0.47	2.79E-02
PSIP1	PC4 and SFRS1-interacting protein (CLL-associated antigen KW-7) (Dense fine speckles 70 kDa protein) (DFS 70) (Lens epithelium-derived growth factor) (Transcriptional coactivator p75/p52)	0.83	2.80E-02
SEPTIN6	Septin-6	0.92	2.84E-02
ACOT9	Acyl-coenzyme A thioesterase 9, mitochondrial (Acyl-CoA thioesterase 9) (EC 3.1.2.-) (Acyl-CoA thioester hydrolase 9)	0.58	2.85E-02
SDHA	Succinate dehydrogenase [ubiquinone] flavoprotein subunit, mitochondrial (EC 1.3.5.1) (Flavoprotein subunit of complex II) (Fp)	0.61	2.88E-02
MYADM	Myeloid-associated differentiation marker (Protein SB135)	0.56	2.89E-02
NTPCR	Cancer-related nucleoside-triphosphatase (NTPase) (EC 3.6.1.15) (Nucleoside triphosphate phosphohydrolase)	0.48	2.89E-02
IDH3B	Isocitrate dehydrogenase [NAD] subunit beta, mitochondrial (Isocitric dehydrogenase subunit beta) (NAD(+)-specific ICDH subunit beta)	0.72	2.89E-02
COPA	Coatomer subunit alpha (Alpha-coat protein) (Alpha-COP) (HEP-COP) (HEPCOP) [Cleaved into: Xenin (Xenopsin-related peptide); Proxenin]	0.64	2.92E-02
SEC63	Translocation protein SEC63 homolog	0.42	2.96E-02
RPN2	Dolichyl-diphosphooligosaccharide--protein glycosyltransferase subunit 2 (Dolichyl-diphosphooligosaccharide--protein glycosyltransferase 63 kDa subunit) (RIBIIR) (Ribophorin II) (RPN-II) (Ribophorin-2)	0.57	2.97E-02
PDIA4	Protein disulfide-isomerase A4 (EC 5.3.4.1) (Endoplasmic reticulum resident protein 70) (ER protein 70) (ERp70) (Endoplasmic reticulum resident protein 72) (ER protein 72) (ERp-72) (ERp72)	0.54	2.99E-02
TSG101	Tumor susceptibility gene 101 protein (ESCRT-I complex subunit TSG101)	0.31	2.99E-02
	cDNA FLJ41538 fis, clone BRTHA2018129	0.63	3.01E-02
PRDX1	Peroxiredoxin-1 (EC 1.11.1.24) (Natural killer cell-enhancing factor A) (NKEF-A) (Proliferation-associated gene protein) (PAG) (Thioredoxin peroxidase 2) (Thioredoxin-dependent peroxide reductase 2) (Thioredoxin-dependent peroxiredoxin 1)	0.38	3.01E-02
DAD1	Dolichyl-diphosphooligosaccharide--protein glycosyltransferase subunit DAD1 (Oligosaccharyl transferase subunit DAD1) (Defender against cell death 1) (DAD-1)	0.65	3.02E-02
YWHAG	14-3-3 protein gamma (Protein kinase C inhibitor protein 1) (KCIP-1) [Cleaved into: 14-3-3 protein gamma, N-terminally processed]	0.35	3.02E-02
SLC2A1	Solute carrier family 2, facilitated glucose transporter member 1 (Glucose transporter type 1, erythrocyte/brain) (GLUT-1) (HepG2 glucose transporter)	0.45	3.11E-02
HMGCL	3-hydroxy-3-methylglutarate-CoA lyase (EC 4.1.3.4) (Hydroxymethylglutaryl-CoA lyase, mitochondrial)	0.49	3.13E-02

EZR	Ezrin (Cytovillin) (Villin-2) (p81)	0.23	3.16E-02
ATP1A1	Sodium/potassium-transporting ATPase subunit alpha-1 (Na(+)/K(+) ATPase alpha-1 subunit) (EC 7.2.2.13) (Sodium pump subunit alpha-1)	0.45	3.16E-02
KIF4A	Chromosome-associated kinesin KIF4A (Chromokinesin-A)	0.69	3.20E-02
SFPQ	Splicing factor, proline- and glutamine-rich (100 kDa DNA-pairing protein) (hPOMp100) (DNA-binding p52/p100 complex, 100 kDa subunit) (Polypyrimidine tract-binding protein-associated-splicing factor) (PSF) (PTB-associated-splicing factor)	0.52	3.23E-02
	F-actin-capping protein subunit beta	0.36	3.28E-02
STX5	Syntaxin-5	0.57	3.29E-02
PPA2	Inorganic pyrophosphatase 2, mitochondrial (EC 3.6.1.1) (Pyrophosphatase SID6-306) (Pyrophosphate phospho-hydrolase 2) (PPase 2)	0.64	3.30E-02
EEF1D	Elongation factor 1-delta (EF-1-delta) (Antigen NY-CO-4)	0.29	3.32E-02
PTGES3	Prostaglandin E synthase 3 (EC 5.3.99.3) (Cytosolic prostaglandin E2 synthase) (cPGES) (Hsp90 co-chaperone) (Progesterone receptor complex p23) (Telomerase-binding protein p23)	0.46	3.32E-02
MAT2A	S-adenosylmethionine synthase isoform type-2 (AdoMet synthase 2) (EC 2.5.1.6) (Methionine adenosyltransferase 2) (MAT 2) (Methionine adenosyltransferase II) (MAT-II)	0.32	3.34E-02
MCAT	Malonyl-CoA-acyl carrier protein transacylase, mitochondrial (MCT) (EC 2.3.1.39) (Mitochondrial malonyl CoA: ACP acyltransferase) (Mitochondrial malonyltransferase) ([Acyl-carrier-protein] malonyltransferase)	0.61	3.35E-02
TBL2	Transducin beta-like protein 2 (WS beta-transducin repeats protein) (WS-betaTRP) (Williams-Beuren syndrome chromosomal region 13 protein)	0.69	3.42E-02
SRPRA	Signal recognition particle receptor subunit alpha (SR-alpha) (Docking protein alpha) (DP-alpha)	0.60	3.45E-02
CNP	2',3'-cyclic-nucleotide 3'-phosphodiesterase (CNP) (CNPase) (EC 3.1.4.37)	0.60	3.47E-02
SNRPA1	U2 small nuclear ribonucleoprotein A' (U2 snRNP A')	0.65	3.47E-02
HNRNPDL	Heterogeneous nuclear ribonucleoprotein D-like (hnRNP D-like) (hnRNP DL) (AU-rich element RNA-binding factor) (JKT41-binding protein) (Protein laAUF1)	0.60	3.47E-02
ACSL3	Fatty acid CoA ligase Acsl3 (Arachidonate--CoA ligase) (EC 6.2.1.15) (Long-chain acyl-CoA synthetase 3) (LACS 3) (Long-chain-fatty-acid--CoA ligase 3) (EC 6.2.1.3) (Medium-chain acyl-CoA ligase Acsl3) (EC 6.2.1.2)	0.55	3.48E-02
YWHAQ	14-3-3 protein theta (14-3-3 protein T-cell) (14-3-3 protein tau) (Protein HS1)	0.51	3.48E-02
ISOC2	Isochorismatase domain-containing protein 2	0.70	3.49E-02
CTNND1	Catenin delta-1 (Cadherin-associated Src substrate) (CAS) (p120 catenin) (p120(ctn)) (p120(cas))	0.53	3.49E-02
SYNCRIP	Heterogeneous nuclear ribonucleoprotein Q (hnRNP Q) (Glycine- and tyrosine-rich RNA-binding protein) (GRY-RBP) (NS1-associated protein 1) (Synaptotagmin-binding, cytoplasmic RNA-interacting protein)	0.45	3.50E-02

MRPL15	39S ribosomal protein L15, mitochondrial (L15mt) (MRP-L15) (Mitochondrial large ribosomal subunit protein uL15m)	0.46	3.51E-02
TARS2	Threonine--tRNA ligase, mitochondrial (EC 6.1.1.3) (Threonyl-tRNA synthetase) (ThrRS) (Threonyl-tRNA synthetase-like 1)	0.64	3.53E-02
SPTAN1	Spectrin alpha chain, non-erythrocytic 1 (Alpha-II spectrin) (Fodrin alpha chain) (Spectrin, non-erythroid alpha subunit)	0.68	3.55E-02
HSD17B10	3-hydroxyacyl-CoA dehydrogenase type-2 (EC 1.1.1.35) (17-beta-estradiol 17-dehydrogenase) (EC 1.1.1.62) (2-methyl-3-hydroxybutyryl-CoA dehydrogenase) (MHBD) (3-alpha-(17-beta)-hydroxysteroid dehydrogenase (NAD(+))) (EC 1.1.1.239) (3-hydroxy-2-methylbutyryl-CoA dehydrogenase) (EC 1.1.1.178) (3-hydroxyacyl-CoA dehydrogenase type II) (3alpha(or 20beta)-hydroxysteroid dehydrogenase) (EC 1.1.1.53) (7-alpha-hydroxysteroid dehydrogenase) (EC 1.1.1.159) (Endoplasmic reticulum-associated amyloid beta-peptide-binding protein) (Mitochondrial ribonuclease P protein 2) (Mitochondrial RNase P protein 2) (Short chain dehydrogenase/reductase family 5C member 1) (Short-chain type dehydrogenase/reductase XH98G2) (Type II HADH)	0.48	3.60E-02
FASTKD1	FAST kinase domain-containing protein 1, mitochondrial	0.38	3.62E-02
EPHX1	Epoxide hydrolase 1 (EC 3.3.2.9) (Epoxide hydratase) (Microsomal epoxide hydrolase) (mEH)	0.70	3.70E-02
CALD1	Caldesmon (CDM)	0.51	3.71E-02
MMUT	Methylmalonyl-CoA mutase, mitochondrial (MCM) (EC 5.4.99.2) (Methylmalonyl-CoA isomerase)	0.48	3.79E-02
ATP2B1	Plasma membrane calcium-transporting ATPase 1 (EC 7.2.2.10) (Plasma membrane calcium ATPase isoform 1) (PMCA1) (Plasma membrane calcium pump isoform 1)	0.49	3.81E-02
WDR74	WD repeat-containing protein 74 (NOP seven-associated protein 1)	0.85	3.82E-02
LPCAT2	Lysophosphatidylcholine acyltransferase 2 (LPC acyltransferase 2) (LPCAT-2) (LysoPC acyltransferase 2) (EC 2.3.1.23) (1-acylglycerol-3-phosphate O-acyltransferase 11) (1-AGP acyltransferase 11) (1-AGPAT 11) (EC 2.3.1.51) (1-acylglycerophosphocholine O-acyltransferase) (1-alkenylglycerophosphocholine O-acyltransferase) (EC 2.3.1.25) (1-alkylglycerophosphocholine O-acetyltransferase) (EC 2.3.1.67) (Acetyl-CoA:lyso-platelet-activating factor acetyltransferase) (Acetyl-CoA:lyso-PAF acetyltransferase) (Lyso-PAF acetyltransferase) (LysoPAFAT) (Acyltransferase-like 1) (Lysophosphatidic acid acyltransferase alpha) (LPAAT-alpha)	0.38	3.84E-02
	IG c1122_heavy_IGHV3-7_IGHD3-3_IGHJ4 (IG c1192_heavy_IGHV3-7_IGHD3-3_IGHJ4) (IG c695_heavy_IGHV3-7_IGHD3-3_IGHJ4) (Fragment)	0.72	3.86E-02
PDIA6	Protein disulfide-isomerase A6 (EC 5.3.4.1) (Endoplasmic reticulum protein 5) (ER protein 5) (ERp5) (Protein disulfide isomerase P5) (Thioredoxin domain-containing protein 7)	0.57	3.89E-02
DSG2	Desmoglein-2 (Cadherin family member 5) (HDGC)	0.40	3.90E-02
RPS19	40S ribosomal protein S19 (Small ribosomal subunit protein eS19)	0.23	3.92E-02

NFIB	Nuclear factor 1 B-type (NF1-B) (Nuclear factor 1/B) (CCAAT-box-binding transcription factor) (CTF) (Nuclear factor I/B) (NF-I/B) (NFI-B) (TGGCA-binding protein)	0.43	3.93E-02
POLR1G	DNA-directed RNA polymerase I subunit RPA34 (A34.5) (Antisense to ERCC-1 protein) (ASE-1) (CD3-epsilon-associated protein) (CD3E-associated protein) (DNA-directed RNA polymerase I subunit G) (RNA polymerase I-associated factor PAF49)	0.65	3.93E-02
PLS3	Plastin-3 (T-plastin)	0.21	3.94E-02
PPIA	Peptidyl-prolyl cis-trans isomerase A (PPIase A) (EC 5.2.1.8) (Cyclophilin A) (Cyclosporin A-binding protein) (Rotamase A) [Cleaved into: Peptidyl-prolyl cis-trans isomerase A, N-terminally processed]	0.44	3.96E-02
LGALS1	Galectin-1 (Gal-1) (14 kDa laminin-binding protein) (HLBP14) (14 kDa lectin) (Beta-galactoside-binding lectin L-14-I) (Galaptin) (HBL) (HPL) (Lactose-binding lectin 1) (Lectin galactoside-binding soluble 1) (Putative MAPK-activating protein PM12) (S-Lac lectin 1)	0.64	3.97E-02
STT3A	Dolichyl-diphosphooligosaccharide--protein glycosyltransferase subunit STT3A (Oligosaccharyl transferase subunit STT3A) (STT3-A) (EC 2.4.99.18) (B5) (Integral membrane protein 1) (Transmembrane protein TMC)	0.45	3.98E-02
CORO1C	Coronin-1C (Coronin-3) (hCRNN4)	0.46	3.98E-02
CTSZ	Cathepsin Z (EC 3.4.18.1) (Cathepsin P) (Cathepsin X)	0.81	4.02E-02
PHGDH	D-3-phosphoglycerate dehydrogenase (3-PGDH) (EC 1.1.1.95) (2-oxoglutarate reductase) (EC 1.1.1.399) (Malate dehydrogenase) (EC 1.1.1.37)	0.27	4.09E-02
ACOX3	Peroxisomal acyl-coenzyme A oxidase 3 (EC 1.3.3.6) (Branched-chain acyl-CoA oxidase) (BRCACox) (Pristanoyl-CoA oxidase)	0.57	4.17E-02
FLNA	Filamin-A (FLN-A) (Actin-binding protein 280) (ABP-280) (Alpha-filamin) (Endothelial actin-binding protein) (Filamin-1) (non-muscle filamin)	0.49	4.17E-02
RPS26	40S ribosomal protein S26 (Small ribosomal subunit protein eS26)	0.37	4.21E-02
RMC1	Regulator of MON1-CCZ1 complex (Colon cancer-associated protein Mic1) (Mic-1) (WD repeat-containing protein 98)	0.54	4.24E-02
FLNB	Filamin-B (FLN-B) (ABP-278) (ABP-280 homolog) (Actin-binding-like protein) (Beta-filamin) (Filamin homolog 1) (Fh1) (Filamin-3) (Thyroid autoantigen) (Truncated actin-binding protein) (Truncated ABP)	0.36	4.27E-02
SLFN5	Schlafen family member 5	0.29	4.28E-02
ATAD1	Outer mitochondrial transmembrane helix translocase (EC 7.4.2.-) (ATPase family AAA domain-containing protein 1) (hATAD1) (Thorase)	0.76	4.28E-02
HSD17B12	Very-long-chain 3-oxoacyl-CoA reductase (EC 1.1.1.330) (17-beta-hydroxysteroid dehydrogenase 12) (17-beta-HSD 12) (3-ketoacyl-CoA reductase) (KAR) (Estradiol 17-beta-dehydrogenase 12) (EC 1.1.1.62) (Short chain dehydrogenase/reductase family 12C member 1)	0.44	4.28E-02
MFN2	Mitofusin-2 (EC 3.6.5.-) (Transmembrane GTPase MFN2)	0.85	4.33E-02
EEF1B2	Elongation factor 1-beta (EF-1-beta)	0.52	4.35E-02

MRPS16	28S ribosomal protein S16, mitochondrial (MRP-S16) (S16mt) (Mitochondrial small ribosomal subunit protein bS16m)	0.47	4.35E-02
NFATC1	Nuclear factor of activated T-cells, cytoplasmic 1 (NF-ATc1) (NFATc1) (NFAT transcription complex cytosolic component) (NF-ATc) (NFATc)	0.85	4.35E-02
DYNLL1	Dynein light chain 1, cytoplasmic (8 kDa dynein light chain) (DLC8) (Dynein light chain LC8-type 1) (Protein inhibitor of neuronal nitric oxide synthase) (PIN)	0.85	4.39E-02
	IGH c241_heavy__IGHV3-15_IGHD3-10_IGHJ4 (Fragment)	1.13	4.40E-02
NR1H4	Bile acid receptor (Farnesoid X-activated receptor) (Farnesol receptor HRR-1) (Nuclear receptor subfamily 1 group H member 4) (Retinoid X receptor-interacting protein 14) (RXR-interacting protein 14)	0.86	4.41E-02
DDX1	ATP-dependent RNA helicase DDX1 (EC 3.6.4.13) (DEAD box protein 1) (DEAD box protein retinoblastoma) (DBP-RB)	0.32	4.46E-02
SRP9	Signal recognition particle 9 kDa protein (SRP9)	0.87	4.48E-02
ATP2A2	Sarcoplasmic/endoplasmic reticulum calcium ATPase 2 (SERCA2) (SR Ca(2+)-ATPase 2) (EC 7.2.2.10) (Calcium pump 2) (Calcium-transporting ATPase sarcoplasmic reticulum type, slow twitch skeletal muscle isoform) (Endoplasmic reticulum class 1/2 Ca(2+) ATPase)	0.40	4.52E-02
MRPL16	39S ribosomal protein L16, mitochondrial (L16mt) (MRP-L16) (Mitochondrial large ribosomal subunit protein uL16m)	0.65	4.56E-02
KANK2	KN motif and ankyrin repeat domain-containing protein 2 (Ankyrin repeat domain-containing protein 25) (Matrix-remodeling-associated protein 3) (SRC-1-interacting protein) (SIP) (SRC-interacting protein) (SRC1-interacting protein)	0.58	4.56E-02
PLD3	5'-3' exonuclease PLD3 (EC 3.1.16.1) (Choline phosphatase 3) (HindIII K4L homolog) (Hu-K4) (Phosphatidylcholine-hydrolyzing phospholipase D3) (Phospholipase D3) (PLD 3)	0.69	4.58E-02
NADK2	NAD kinase 2, mitochondrial (EC 2.7.1.23) (Mitochondrial NAD kinase) (NAD kinase domain-containing protein 1, mitochondrial)	0.55	4.63E-02
EFNB2	Ephrin-B2 (EPH-related receptor tyrosine kinase ligand 5) (LERK-5) (HTK ligand) (HTK-L)	0.87	4.64E-02
RPLP1	60S acidic ribosomal protein P1 (Large ribosomal subunit protein P1)	0.20	4.67E-02
TIMM44	Mitochondrial import inner membrane translocase subunit TIM44	0.60	4.70E-02
CORO2A	Coronin-2A (IR10) (WD repeat-containing protein 2)	0.57	4.71E-02
	cDNA FLJ26613 fis, clone MPB05565, highly similar to Serine/threonine protein phosphatase 2A, 55 kDa regulatory subunit B, alpha isoform	0.49	4.71E-02
EIF2S3	Eukaryotic translation initiation factor 2 subunit 3 (EC 3.6.5.3) (Eukaryotic translation initiation factor 2 subunit gamma X) (eIF-2-gamma X) (eIF-2gX)	0.35	4.74E-02
HNRNPH1	Heterogeneous nuclear ribonucleoprotein H (hnRNP H) [Cleaved into: Heterogeneous nuclear ribonucleoprotein H, N-terminally processed]	0.45	4.76E-02
PTBP3	Polypyrimidine tract-binding protein 3 (Regulator of differentiation 1) (Rod1)	0.47	4.79E-02
UFM1	Ubiquitin-fold modifier 1	0.83	4.80E-02

ITPR1	Inositol 1,4,5-trisphosphate receptor type 1 (IP3 receptor isoform 1) (IP3R 1) (InsP3R1) (Type 1 inositol 1,4,5-trisphosphate receptor) (Type 1 InsP3 receptor)	0.63	4.82E-02
PITRM1	Presequence protease, mitochondrial (hPreP) (EC 3.4.24.-) (Pitrilysin metalloproteinase 1) (Metalloprotease 1) (hMP1)	0.52	4.85E-02
CD9	CD9 antigen (5H9 antigen) (Cell growth-inhibiting gene 2 protein) (Leukocyte antigen MIC3) (Motility-related protein) (MRP-1) (Tetraspanin-29) (Tspan-29) (p24) (CD antigen CD9)	0.66	4.89E-02
KIFC1	Kinesin-like protein KIFC1 (Kinesin-like protein 2) (Kinesin-related protein HSET)	0.70	4.90E-02
LGALS3BP	Galectin-3-binding protein (Basement membrane autoantigen p105) (Lectin galactoside-binding soluble 3-binding protein) (Mac-2-binding protein) (MAC2BP) (Mac-2 BP) (Tumor-associated antigen 90K)	1.11	4.90E-02
HNRNPA2B1	Heterogeneous nuclear ribonucleoproteins A2/B1 (hnRNP A2/B1)	0.68	4.92E-02
IGHV3OR16-13	Immunoglobulin heavy variable 3/OR16-13 (non-functional) (Fragment)	0.88	4.93E-02

Table S1.

All significantly enhanced proteins associated with the trapped precursor.

Movie S1.

Full time-lapse movie showing the transfer of healthy mitochondria (MitoTracker Green; green) within a TNT into a cell with trapped precursor (*Su9-mScarlet-DHFR* (magenta) +100 nM MTX). Cells were imaged live using an Olympus IXplore SpinSR system. Each timeframe is a Max z-projection of 10 slices, taken every 5 minutes with 10 timepoints.